

# Impact of Compound Flood Event on Coastal Critical Infrastructures Considering Current and Future Climate

Mariam Khanam<sup>1</sup>, Giulia Sofia<sup>1</sup>, Marika Koukoulas<sup>1</sup>, Rehenuma Lazin<sup>1</sup>, Efthymios I. Nikolopoulos<sup>2</sup>, Xinyi Shen<sup>1</sup>, and Emmanouil N. Anagnostou<sup>1</sup>

<sup>1</sup>Civil and Environmental Engineering, University of Connecticut, Storrs, CT 06269, USA

<sup>2</sup>Mechanical and Civil Engineering, Florida Institute of Technology, Melbourne, FL 32901, USA

*Correspondence to:* Anagnostou, Emmanouil N. (emmanouil.anagnostou@uconn.edu)

**Abstract.** The changing climate and anthropogenic activities raise the likelihood of damages due to compound flood hazards, triggered by the combined occurrence of extreme precipitation and storm surge during high tides, and exacerbated by sea-level rise (SLR). Risk estimates associated with these extreme event scenarios are expected to be significantly higher than estimates derived from a standard evaluation of individual hazards. In this study, we present case studies of compound flood hazards affecting critical infrastructure (CI) in coastal Connecticut (USA). We based the analysis on actual and synthetic (considering future climate conditions for the atmospheric forcing, sea-level rise, and synthetic forecasted hurricane tracks) hurricane events, represented by heavy precipitation and surge combined with tides and SLR conditions. We used the Hydrologic Engineering Center's River Analysis System (HEC-RAS), a two-dimensional hydrodynamic model to simulate the combined coastal and riverine flooding on selected CI sites. We forced a distributed hydrological model (CREST-SVAS) with weather analysis data from the Weather Research and Forecasting (WRF) model for the synthetic events and from the National Land Data Assimilation System (NLDAS) for the actual events, to derive the upstream boundary condition (flood wave) of HEC-RAS. We extracted coastal tide and surge time series for each event from the National Oceanic and Atmospheric Administration (NOAA) to use as the downstream boundary condition of HEC-RAS. The significant outcome of this study represents the evaluation of changes in flood risk for the CI sites for the various compound scenarios (under current and future climate conditions). This approach offers an estimate of the potential impact of compound hazards relative to the 100-year flood maps produced by the Federal Emergency Management Agency (FEMA), which is vital to developing mitigation strategies. In a broader sense, this study provides a framework for assessing the risk factors of our modern infrastructure located in vulnerable coastal areas throughout the world.

## 1 Introduction

The impacts of hurricanes such as Harvey, Irma, Sandy, Florence, and Laura are characteristic examples of hazardous storms that have affected the society and environment of coastal areas and have damaged infrastructure, through the combination of heavy rain and storm surge. The increased frequency of such events raises concerns about compound flood hazards previously considered independent of one another (Barnard et al., 2019; Leonard et al., 2014; Moftakhari et al., 2017; Wahl et al., 2015; Zscheischler et al., 2018; Winsemius et al., 2013; Hallegatte et al., 2013; de Bruijn et al., 2017; de Bruijn et al., 2019; Bevacqua et al., 2019).

Formatted: Font color: Black

Formatted: Normal, Border: Top: (No border), Bottom: (No border), Left: (No border), Right: (No border), Between : (No border), Tab stops: 3.15", Centered + 6.3", Right

Style Definition: Normal

Style Definition: Bullets: Outline numbered + Level: 1 + Numbering Style: 1, 2, 3, ... + Start at: 1 + Alignment: Left + Aligned at: 0" + Tab after: 0.5" + Indent at: 0.5"

Style Definition: Revision: Justified, Line spacing: 1.5 lines

Formatted

Formatted: Font color: Black

Formatted: Normal, Space Before: 9 pt, Border: Top: (No border), Bottom: (No border), Left: (No border), Right: (No border), Between : (No border)

Formatted: Font color: Black, English (United Kingdom)

Formatted: Font color: Black

Formatted: Normal, Border: Top: (No border), Bottom: (No border), Left: (No border), Right: (No border), Between : (No border), Tab stops: 3.13", Centered + 6.27", Right

Formatted: Font color: Black

Formatted: Normal, Border: Top: (No border), Bottom: (No border), Left: (No border), Right: (No border), Between : (No border), Tab stops: 3.15", Centered + 6.3", Right

36 Concurrent with the rise in event intensities, ~~the elevated damage and disruptions~~ caused by compound flooding (CF)  
37 to critical infrastructure (CI) and services ~~have substantial adverse socioeconomic impacts. Low-lying coastal areas,~~  
38 ~~where almost 40 percent of people in the United States live (NOAA, 2013), are especially vulnerable to CF threats to~~  
39 ~~infrastructures such as~~ ~~including~~ electrical systems, water, and sewage treatment facilities, and other utilities that  
40 underpin modern society. ~~have substantial adverse socioeconomic impacts, especially in low-lying coastal areas,~~  
41 ~~where almost 40 percent of people in the United States live (NOAA, 2013).~~

42 The growing record of significant impacts from extreme events around the world (Chang et al., 2007; McEvoy et al.,  
43 2012; Ziervogel et al., 2014; FEMA, 2013; Karagiannis et al., 2017) adds ~~an~~ urgency to the need for reassessing  
44 CI management policies based on compound impact, to help ensure flood safety and rapid emergency management  
45 (Pearson et al., 2018). The uncertainty of the current evolution of compound events translates into an even  
46 ~~greater~~larger uncertainty concerning future damage to CI (de Bruijn et al., 2019, Marsooli et al., 2019).

47 Recent studies have underlined the importance of understanding and quantifying the flood impacts on critical  
48 infrastructure, and their broader implications in risk management and catchment-level planning (Chang et al., 2007;  
49 McEvoy et al., 2012; Ziervogel et al., 2014; de Bruijn et al., 2019; Pearson et al., 2018; Pant et al., 2018; Dawson,  
50 2018). Some authors have estimated the frequency of compound flooding and provide approaches to risk assessment  
51 based on the joint probability of precipitation and surge (Bevacqua et al., 2019; Wahl et al., 2015). The spatial extent  
52 and depth of compound flooding can vary in frequency (Quinn, et al., 2019) if any of the components of CF is not  
53 taken into consideration while evaluating flood frequency. Both storm surges and heavy precipitation, and their  
54 interplay, are likely to change in the future (Field et al., 2012, Dottori et al., 2018; Blöschl et al., 2017; Muis et al.,  
55 2016; Marsooli et al., 2019; Vousdoukas et al., 2018). Nonetheless, the effects of CF, considering the climate change  
56 impact, have not been thoroughly explored yet.

57  
58 To deal with CF threats and challenges to coastal communities, there is a need to develop efficient frameworks for  
59 performing systematic risk analysis based on a wide range of actual and what-if scenarios of such events in current  
60 and future climate conditions. In this study, we focused on coastal power grid substations as critical infrastructure and  
61 investigated the impacts of compound flood hazard scenarios associated with tropical storms. We present a hydrologic-  
62 hydrodynamic modeling framework to evaluate the integrated impact of flood drivers causing CF by ~~synthesizing~~  
63 ~~synthesizing~~ current and future scenarios. This study enables the quantitative measurement of CF hazard ~~easteds cast~~  
64 on critical infrastructures in terms of flood depth and flood extent by observing actual storm-induced floods and  
65 drawing information from synthetic scenarios. To project the combined flood hazard in future climate conditions, we  
66 integrated the effects of SLR, tides, and synthetic hurricane event simulations into the flood hazard exposure.

67 Even though past research on the assessment of damages to the power system components or other related  
68 infrastructures has proposed design and operation countermeasures and remedies ( ~~i.e.:~~ Kwasinski et al. 2009; Reed  
69 et al. 2010; ~~Abi-Sarraf Samra~~ and Henry, 2011; Chang et al., 2007; de Bruijn et al., 2019; Pearson et al., 2018;  
70 Pant et al., 2018; Dawson, 2018), these studies lack a comprehensive hazard assessment on power grid components,  
71 and ~~potential changes due to climate change.~~

72 The scenario-based analysis of this study formed the basis on which to address two questions:

Formatted: Font color: Black

Formatted: Normal, Border: Top: (No border), Bottom: (No border), Left: (No border), Right: (No border), Between : (No border), Tab stops: 3.13", Centered + 6.27", Right

Formatted: Font color: Black

Formatted: Normal, Border: Top: (No border), Bottom: (No border), Left: (No border), Right: (No border), Between : (No border), Tab stops: 3.15", Centered + 6.3", Right

73 (1) What are the characteristics of the tropical storm-related inundation, considering the compound effect of riverine  
74 and coastal flooding coinciding or not with peak high tides  
75 (2) Will future climate (including SLR and intensification of storms due to warmer sea surface temperatures) bring a  
76 significant increase in flood impact for the power-grid coastal infrastructures?

77 The proposed framework offers a multi-dimensional strategy to quantify the potential impacts of tropical storms, thus  
78 enabling ~~for~~ a more resilient grid for climate change and the increasing incidence of severe weather.  
79 We investigated these questions based on eight case studies of CI in Connecticut (USA), distributed on the banks of  
80 coastal rivers discharging along the Long Island Sound.

## 81 2 Materials and methods

### 82 2.1 Study sites

83 This study focused on seven coastal river reaches (Fig. 1, Table 1), where eight power grid substations lie in proximity  
84 to riverbanks and are prone to flooding caused by both coastal storms (such as hurricanes) that combine heavy  
85 precipitation and high surge. These power grid substations are ~~eoded~~labeled on the map CII through CI8.

86 For each river reach adjacent to a CI, we developed a hydrodynamic model domain, and we applied a distributed  
87 hydrological model for predicting river flows from the upstream river basin. Table 1 shows the specification of each  
88 river reach, associated drainage basin, the correspondent domain extent for the hydrodynamic simulations, and the  
89 hydrological distance [distance along the flow paths] of each power grid substation from the coastline. This distance  
90 was derived using the 30m National Elevation Dataset (NED) for the continental United States (USGS 2017).

91 Among the case study sites, two CIs are relatively inland [CI3 and CI4] (table 1: see hydrologic distance. Figure 1:  
92 see coastal boundary), nonetheless all the sites are included within the Coastal Area as defined by Connecticut General  
93 Statute (CGS) 22a-94(a) [[https://www.cga.ct.gov/current/pub/chap\\_444.htm#sec\\_22a-94](https://www.cga.ct.gov/current/pub/chap_444.htm#sec_22a-94)]. The ~~\_\_\_\_\_~~ considered rivers  
94 belong to watersheds ranging from 10 to 300 km<sup>2</sup> basin area, which are sub-basins of the Connecticut River basin.  
95 The hydrodynamic model simulation domains ranged from 3.7 to 8.3 km in river length and 2.2 and 20.7 km<sup>2</sup> in area.

### 96 2.2 Simulation framework

97 To evaluate the effect of compound events, we selected four tropical storms: two actual hurricanes (Sandy and Irene)  
98 that hit Connecticut, and two synthetic scenarios based on actual hurricanes Sandy and Florence. Both Irene (August  
99 21–28, 2011) and Sandy (October 22–November 2, 2012) reached category 3, but they made landfall in Connecticut  
100 as category 1 hurricanes. The synthetic simulations (Chapt. 2.2.1) include different atmospheric conditions leading to  
101 landfall scenarios with ~~greater~~more significant impacts. The Sandy synthetic scenario represents hurricane Sandy  
102 under future climate and sea surface conditions (Lackmann 2015), while the synthetic scenarios for Florence were  
103 based on simulated surge-tide conditions and future SLR (see Chapt. 2.2.1 and 2.3).

104 To investigate the impact of floods of the various scenarios, we devised a combined hydrological (Chapt. 2.2.2) and  
105 hydrodynamic (Chapt. 2.2.3) modeling framework (Figure 2), forced with weather reanalysis and geospatial data for

Formatted: Font color: Black

Formatted: Normal, Border: Top: (No border), Bottom: (No border), Left: (No border), Right: (No border), Between : (No border), Tab stops: 3.13", Centered + 6.27", Right

106 the actual events, and a numerical weather prediction model (subsection a) for the synthetic events (that is, synthetic  
107 hurricane Florence and future hurricane Sandy).

### 108 2.2.1 Atmospheric simulations

109 To simulate the two synthetic Sandy and Florence hurricane events, we used the Weather Research and Forecasting  
110 (WRF) system (Powers et al., 2017; [ShamarockSk\\_amarock](#) et al., 2007). For the synthetic hurricane Florence event,  
111 we used a hurricane track forecast by the National Oceanic and Atmospheric Administration (NOAA), that as of  
112 September 6, 2018, according to the Global Forecast System (GFS) forecasts of the National Center for Environmental  
113 Prediction (NCEP), showed landfall in Long Island and Connecticut on September 14 as a category 1 hurricane  
114 (Higgins 2000).

115 We based synthetic hurricane Sandy events on future climate conditions (post-2100).

116 For the soil type and texture input in the WRF model for both synthetic storm simulations, we used the USGS  
117 GMTED2010 30-arc-second (Danielson and Gesch 2011) Digital Elevation Model for the topography, the Noah-  
118 modified 21-category IGBP-MODIS (Friedl et al., 2010) for land use, and vegetation input, and the Hybrid  
119 STATSGO/FAO (30-second) (FAO 1991) for soil characteristics.

120 To simulate the synthetic hurricane Florence with WRF, we used the GFS forecasts at  $0.25^\circ \times 0.25^\circ$  spatial resolution  
121 as initial and boundary conditions. We used a three-grid setup with a coarse external domain of 18 km spatial resolution  
122 and two nested domains with 6 km and 2 km horizontal grid spacing, respectively. Two-way nesting was activated for  
123 both inner domains. Vertically, the domains stretched up to 50 mb with 28 layers. We parameterized convective  
124 activity on the outer (resolution of 18 km) and the first nested (resolution of 6 km) domain using the Grell 3D ensemble  
125 scheme (Grell and Devenyi 2002). Further details on the model setup are presented in Table 2.

126 For the future hurricane Sandy scenario, we used the hurricane Sandy simulations under future climate conditions  
127 (after 2100) by Lackman (2015), who used a three-grid setup at spatial resolutions of 54, 18, and 6 km. We defined  
128 initial and boundary conditions by altering the European Centre for Medium-Range Weather Forecasts (ECMWF)  
129 interim reanalysis (Dee et al., 2011) data, based on five General Circulation Model (GCM)-projected, late-century  
130 thermodynamic changes derived from the IPCC (Intergovernmental Panel on Climate Change) AR4 A2 emissions  
131 scenario (Meehl et al., [20172007](#)). A complete description of the modeling framework is provided by Lackman  
132 (2015).

### 133 2.2.2 Hydrological modeling

134 To account for the river inflow (upstream boundary condition), we applied a physically-based distributed hydrological  
135 model [CREST-SVAS (Coupled Routing and Excess Storage–Soil–Vegetation–Atmosphere–Snow)] described in  
136 Shen and Anagnostou (2017).

137 To simulate river discharges for the synthetic hurricanes (Florence and future Sandy), we used the WRF simulations  
138 at 6-km/hourly spatiotemporal resolution, as described above. To force the hydrological model for the actual events  
139 (Sandy and Irene), we used data from Phase 2 of the North American Land Data Assimilation System (NLDAS-2)  
140 (Xia et al., 2012) dataset. NLDAS-2 is a gridded dataset derived from bias-corrected reanalysis and in situ observation

Formatted: Font color: Black

Formatted: Normal, Border: Top: (No border), Bottom: (No border), Left: (No border), Right: (No border), Between : (No border), Tab stops: 3.15", Centered + 6.3", Right

Formatted: Font color: Black

Formatted: Normal, Border: Top: (No border), Bottom: (No border), Left: (No border), Right: (No border), Between : (No border), Tab stops: 3.13", Centered + 6.27", Right

141 data, with a one-eighth-degree grid resolution and an hourly temporal resolution, available from January 1, 1979, to  
142 the present day. We derived the precipitation from daily rain gauge data over the continental United States, and all  
143 other forcing data came from the North American Regional Reanalysis (NARR) by NCEP (Higgins 2000), to which  
144 we applied bias and vertical corrections. To reduce the computational effort, we performed the hydrological simulation  
145 using a hydrologically conditioned 30 m spatial resolution DEM (USGS 2017).

146 The hydrologic simulation includes the use of land use and land cover information retrieved from the Moderate  
147 Resolution Imaging Spectroradiometer (“MOD12Q1” from MODIS) (Friedl et al., 2015). To compensate for the  
148 coarse resolution (500 m) of these data, we obtained imperviousness ratios using Connecticut’s Changing Landscape  
149 (CCL) database and the National Land Cover Database (NLCD) at 30 m resolution. In CREST-SVAS, the land surface  
150 process was simulated by solving the coupled water and energy balances to generate streamflow at hourly time steps  
151 at the outlet of the studied watershed. CREST-SVAS was calibrated and validated for the whole Connecticut river  
152 basin [that contains all the investigated sites] with an NSCE of 0.63 (Shen and Anagnostou, 2017). We further  
153 validated the model considering hourly flows in two locations within the Housatonic River and Naugatuck River  
154 watersheds with an NSCE of 0.69 (Hardesty et al., 2018). The quality measures indicate a satisfactory model  
155 performance at the watershed scale over the topographic region that collectively include our study sites.

### 156 2.2.3 Hydrodynamic modeling

157 To assess the flood hazard in terms of extent and the maximum depth of the flood, we implemented the Hydrologic  
158 Engineering Center’s River Analysis System (HEC-RAS), developing two-dimensional model domains around the CI  
159 location. Except for CI4 and CI5, which are within the same simulation domain, each substation has an independent  
160 domain.

161 The inundation maps are derived using a 1m LIDAR DEM (CtECO 2016) taken as base maps for the study reaches.  
162 To better represent the impacts of urban establishments on inundation dynamics, solid urban features such as houses  
163 and buildings, which obstruct the flow of stormwater, were added to the bare-earth DEM. For this, we considered the  
164 building footprints from (CtECO, 2012) and identified positions of buildings and houses in the DEM by increasing  
165 the elevation of the pixels within the building footprint polygons by an arbitrary height of 4.5 m, assuming one-story  
166 buildings.

167 The considered locations have no bathymetric (underwater topography) data represented in the DEM. In general, the  
168 impact of inclusion/exclusion of bathymetry data on the hydrodynamic model simulations will vary according to the  
169 river size and event severity (Cook & Merwade 2009). For the investigated events in this study, flood risk is mainly  
170 dominated by defence overflow and defence breaching. The proposed analysis focussed upon the effects of extreme  
171 events that are so severe that all defences would, in any case, be overtopped. This means that we do not require allows  
172 for a simplification of the modelling problem and allows for a correct approximation of flows even without detailed  
173 bathymetric information in the upstream main channel, thereby considerably simplifying the modeling problem as  
174 underlined in (Bates et al. 2013). Therefore, we did not represent the flow of water in the main channel. Rather  
175 boundary conditions were given as time series of water surface elevation imposed along the defence crests, 2005).

Formatted: Font color: Black

Formatted: Normal, Border: Top: (No border), Bottom: (No border), Left: (No border), Right: (No border), Between : (No border), Tab stops: 3.15", Centered + 6.3", Right

Formatted: Font color: Black

Formatted: Normal, Border: Top: (No border), Bottom: (No border), Left: (No border), Right: (No border), Between : (No border), Tab stops: 3.13", Centered + 6.27", Right

176 To reduce the computation time, we created a 2D mesh grid at 10 m background resolution, enforced with breaklines  
177 to intensify the riverbank and other areas with a large elevation gradient up to 1 m resolution. ~~The CREST-SVAS~~  
178 ~~provided the~~ upstream boundary condition ~~was~~. ~~National Water Level Observation Network (NWLON) data,~~  
179 ~~provided by CREST-SVAS, and NOAA, offered the basis for defining~~ the downstream boundary condition (coastal  
180 water level, including coastal tide, storm surge, and sea level) ~~was derived from National Water Level Observation~~  
181 ~~Network (NWLON) data, provided by NOAA. These). The latter~~ data are available as actual observations and  
182 predictions at intervals of six minutes to one hour. Figure 3 provides an example of one of the sites, showing the  
183 upstream and downstream boundaries, along with a map overlay of flooded areas of five (SD1–SD5) scenarios (see  
184 below) for CI2. We initiated the simulation with a warmup period of 12 hours to achieve stability. We chose the full  
185 momentum scheme in HEC-RAS and extracted hourly output from the simulation.

186 The model parameters were calibrated to obtain realistic water depths and extents, as compared to reference data  
187 collected for Sandy. To validate the hydrodynamic model simulations, we used surveyed HWMs (high water marks)  
188 (Koenig et al., 2016) collected by the United States Geological Survey (USGS) after hurricane Sandy at 15 selected  
189 locations spread across the simulation domains. HWMs are frequently used to calibrate and validate model outputs  
190 and satellite-based observations of flood depth (Bunya et al., 2010; Cañizares and Irish 2008; Cariolet, 2010;  
191 Chang et al., 2007; Hostache et al. 2009; McEvoy et al., 2012; Pearson et al., 2018; Schumann et al., 2008;  
192 Schumann et al., 2007a; Schumann et al., 2007b; Ziervogel et al., 2014). As for the flood extent, we further validated  
193 the model against the most accurate available information on the 2D extent, and the maximum depth of storm surge  
194 for Sandy (FEMA, CT DEEP, 2013), created from field-verified HWMs and Storm Surge Sensor data from the  
195 USGS.

196 An HWM does not necessarily indicate the maximum flood depth; rather, it can be a mark from a lower depth that  
197 lasts long enough to leave a trail. Based on this understanding, we compared the HWMs against the simulated flood  
198 depths within a 10x10m radius around the high water marks, also to avoid issues due to the presence of buildings in  
199 the DEM (Boxplots in Fig. 4). The simulated depths demonstrated reasonable agreement with the collected HWM  
200 values (Figure 4), with the model showing a slight overestimation. In this case, the systematic error fell within values  
201 of expected precision, implying a consistent positive bias in the simulations not strong enough to hinder the results.

202 Figure 5 shows a visual comparison for CI1 and CI2 between the simulated inundation (Fig.5 a, c), and the reference  
203 extent (Fig. 5 d,e). A slight overestimation of the flood level, ranging between 0.2 and 0.4 m, with a precision of 0.2  
204 m or less, is observed for the inundation depths at the displayed locations, which is consistent with the results obtained  
205 locally, at the HWM locations (Fig. 4). Taking into consideration the accuracy of the inundation depth, the declared  
206 DEM accuracy (vertical RMSE ~0.3m), and the simplified modeling problem concerning bathymetry, the accuracy of  
207 the flood extent assessment was judged satisfactory.

208

### 209 2.3 Compound scenarios

210 We modeled four types of synthetic compound event scenarios, as well as actual events by (1) simulating the synthetic  
211 hurricanes; (2) introducing a climate change factor, in the form of SLR (~0.6 m), as projected for 2050, as a prediction

Formatted: Font color: Black

Formatted: Normal, Border: Top: (No border), Bottom: (No border), Left: (No border), Right: (No border), Between : (No border), Tab stops: 3.15", Centered + 6.3", Right

Formatted: Font color: Black

Formatted: Normal, Border: Top: (No border), Bottom: (No border), Left: (No border), Right: (No border), Between : (No border), Tab stops: 3.13", Centered + 6.27", Right

for intermediate low probability (CIRCA 2017; O'Donnell, 2020); (3) shifting the surge timing to make the surge peak-level occurring at local high tide; and (4) combining the SLR with the high tide condition. The combination of these four event types yielded nine simulations, hereby coded as IR or SD for hurricanes Irene and Sandy, and FL for the synthetic hurricane Florence.

Two scenarios were created for hurricane Irene. IR1 was the actual hurricane Irene, that made landfall in Connecticut during high tide, and IR2 was the IR1 scenario with future SLR added to the tidal water level as a downstream boundary condition in HEC-RAS.

For hurricane Sandy, we generated five scenarios. SD1 was the actual Sandy. For SD2, we shifted the peak high tide to coincide with the maximum storm surge recorded, as derived from the local NOAA stations (hereafter referred to as 'shifted tide water levels'). We further added SLR to the shifted tide water levels from SD2 to create the third scenario (SD3). The remaining two scenarios for hurricane Sandy represented future climate conditions. Specifically, SD4 was the future hurricane scenario simulated with the GFS (Chapt. 2.2.1) and shifted tidal water level. SD5 was the future Sandy with shifted tide water levels and SLR.

For the synthetic hurricane Florence event, we simulated two scenarios. FL1 was the synthetic Florence event, based on the GFS track that gave landfall in Connecticut and Long Island (Chapt. 2.2.1). FL2 was the same synthetic event, with SLR added to the coastal water levels.

Table 3 shows, for each scenario, the basin-averaged event accumulated precipitation (mm) and the simulated peak flow (m<sup>3</sup>/s) used as an upstream boundary condition in HEC-RAS, along with the recurrence interval of the peak flows derived using a Log-Pearson probability distribution fitted using yearly maxima from the long-term simulated flows (1979-2019) from CREST. This shows how significant the precipitation forcing was for each considered scenario. For CI1, for example, the future Sandy (SD4/5) scenario, with a peak flow of 242.4 m<sup>3</sup>/s, was the most extreme event with a recurrence interval of 316 years, followed by Irene (158.5 m<sup>3</sup>/s) and Florence (51.3m<sup>3</sup>/s) with a recurrence interval of 56 and 2 years respectively, whereas, for CI8, Florence and future Sandy had similar magnitudes with peak flows of 93.1m<sup>3</sup>/s (6) and 94.7m<sup>3</sup>/s (6), respectively. In table 3, we have summarised the maximum total water level (tide & surge) used in the model at the downstream of the study sites for all the scenarios. This table represents the change in the severity of the coastal component of the compound scenarios concerning added challenges like shifted tide and SLR. For example, for CI3, the total water level increases 1m with the shifted tide (SD2/ SD4), and with SLR it becomes 4.4 m.

#### 2.4 Compound flood hazard analysis

We investigated the compound effect of the different events by comparing flood area extents and flood depths for each event. For the flood area extent, we used as a baseline the 100-year flood maps provided by FEMA. [TheWe considered the](#) distance correlation index (dCorr) (Székely et al; 2007) [has been used](#) to identify the correlation of the differences between simulated and FEMA extent and compound events' parameters [flow and total water level peak]. dCorr values range from 0 to 1 expressing the dependence between two independent variables. The closer [the valuedCorr is](#) to 1 [is](#) the stronger the dependency would be, and zero implies that the two variables in question are

Formatted: Font color: Black

Formatted: Normal, Border: Top: (No border), Bottom: (No border), Left: (No border), Right: (No border), Between : (No border), Tab stops: 3.15", Centered + 6.3", Right

Formatted: Font color: Black

Formatted: Normal, Border: Top: (No border), Bottom: (No border), Left: (No border), Right: (No border), Between : (No border), Tab stops: 3.13", Centered + 6.27", Right

247 statistically independent. dCorr can depict the non-monotonic associations of the variables and declare the dCorr value  
248 is zero if only the variables are statistically independent.

249 For the flood level differences, we considered the overall distribution of water depths across the domain of the CI sites  
250 and investigated the time series of water depth at each location (Figure 6 is an example of the simulated flood depth  
251 during the scenarios of Sandy (SD1- SD5) over time for CI2).

252 To evaluate the flood hazard in terms of flood depth, we computed a Cumulative Distribution Function (CDF) to  
253 shows the probability that the flood depth will attain a value less than or equal to each measured value. We estimated  
254 the CDF using all the depth values of all the grid of [the](#) simulation domain, for the time step when the inundation was  
255 maximum. We evaluated the depth empirical exceedance probability (Hanman et al., 2016; Lin et al., 2016; Warner  
256 and Tissot 2012) within the whole domain, considering the maximum depth at each pixel, as suggested in (Pasquier  
257 et al. 2019, Hamman et al. 2016). The benefits of this empirical approach are that it overcomes sensitivity to the  
258 choice of the distribution and does not require a definition of the distribution parameters. By comparing the empirical  
259 distributions, we can investigate how changes in the scenario characteristics modify the frequency of the maximum  
260 inundation depths.

261 The study further looked at whether the depth of water at a station would change for various scenarios. Figure 6 shows  
262 an example of the flood depth over simulated time at CI3 for the scenarios of Sandy. [PreWe investigated pre](#)-defined  
263 [critical/hazardous](#) water levels ~~were investigated~~ for each station, as hypothetical values representing the height  
264 between the floor and the critical electric system in the station. Specifically, we considered 0.5 m, 1.5 m, and 2.5 m  
265 for threshold levels. As a measure of the potential threat to the electric infrastructure, we determined the percentage  
266 of time that the flood level was over each specific threshold (Figure 7-9). This data was then used to assess potential  
267 flooding problems associated with on-site inundation: we associated the changes in risk posed to the CI from the  
268 different examined scenarios based on the changes in those percentages.

### 269 3 Results and Discussion

#### 270 3.1 Flood extent

271 The inundation extents shown in figure 6 represent an aggregation of the overall runs rather than a specific simulation  
272 time, and it represents the extent reached when all pixels had the maximum inundation depth. Total flood extent ranged  
273 between less than 1 km<sup>2</sup> to more than 7 km<sup>2</sup>, with a minimum extent of 0.4 km<sup>2</sup> for the actual Sandy (SD1) at C8, and  
274 a maximum extent of 7.1 km<sup>2</sup> for the future Sandy (SD5) at C3. The results showed consistent agreement that the  
275 flood extent increased with increasing intensity of the event and an increase in the recurrence intervals of the flows  
276 (Table 3).

277 Changes across the study sites relative to the FEMA 100-year flood extend (Table 4, Figure 7a-c) ranged from -87.8%  
278 (for CI8 for SD1) to 192.2% (for CI2 for IR2). Overall, the sites with a return period of fewer than 100 years, showed  
279 consistently less flooding than that of the FEMA map, a finding best represented by the comparison of actual events,  
280 such as IR1.

Formatted: Font color: Black

Formatted: Normal, Border: Top: (No border), Bottom: (No border), Left: (No border), Right: (No border), Between : (No border), Tab stops: 3.15", Centered + 6.3", Right

Formatted: Font color: Black

Formatted: Normal, Border: Top: (No border), Bottom: (No border), Left: (No border), Right: (No border), Between : (No border), Tab stops: 3.13", Centered + 6.27", Right



281 Since the model performance shows a good agreement with the actual flood extent~~extent~~, and the HWMs  
282 (Chapt.2.2.3), our results suggest that FEMA's flood maps do not fully capture the flood extent at least for some  
283 locations. Similar findings were reported in Jordi et al. (2019), Wang et al. (2014), and Xian et al. (2005(2015)),  
284 where tens of meter-scale absolute differences were found between the FEMA estimated flood extent for hurricane  
285 Sandy. The strength of correlation (dCorr) between changes in the upstream (flow peak) or downstream (surge peak)  
286 components, and the absolute differences with FEMA extent, gives an idea of the importance of ~~each~~ every single  
287 driver of change. For the cases investigated in this study, the percentage difference mostly depends on the surge:  
288 surge height explains more than 80% of the variation in the differences to FEMA extent (dcorr=0.8 in median). CI6  
289 appears to be the sites where the surge has the strongest correlation with the absolute difference in flood extent, as  
290 compared to FEMA maps. The differences with FEMA maps are less related to the peak flows (median correlation  
291 0.5, with max correlation recorded for CI3). As expected, the correlation with surge increases at the decreasing of the  
292 hydrologic distance to the coast, while the correlation with the flow increases the further a site is from the coast, even  
293 though this relationship is not linear.

294 As we proceeded with the synthetic scenarios, adding compound and future climate, the results indicated the additional  
295 impacts of the joint flood drivers (shifted tide, surge, SLR).

296 For the same event, peak storm-tide levels occurring near local high tide (i.e., SD2) resulted in more flooding than  
297 that of events happening at low-tide (like actual Sandy, SD1). Climate change related SLR exacerbates extreme  
298 event inundation relative to a fixed extent (FEMA) with variability that ranged from 8.3% (CI4/5) to as high as 425%  
299 (CI8). CI8 is the site hydrologically closer to the coast (see the hydrologic distance in Table 1), making it the most  
300 susceptible to the altered scenario. Nonetheless, the shifted tide increased the inundation relative to the FEMA 100-  
301 year flood map also for CI2 and CI4/5.

302 The effects of compound events emerged drastically with the combination of both shifted tide and SLR. ~~With the~~  
303 ~~exception of~~ Except for CI3 and CI8, all other CIs showed an increase in the percentage change from FEMA (Table  
304 4). In comparison to SD1, SD3 exhibited increased inundation for all the CIs. The inundated area was about 146%  
305 more (1.9 km<sup>2</sup>) for SD3 than SD1 (0.9 km<sup>2</sup>) for CI1, for example. The river flood peak for hurricane Sandy had a  
306 recurrence interval of about two years, but the flood hazard associated with this event became more devastating if  
307 simulated in a compound way, including SLR and shifted tide. This result suggests that events of lower river flood  
308 severity (from ~~less~~ fewer rain accumulations) can produce an aggravating impact, as the intensity of major storm  
309 surges increases due to shifted timing and SLR.

310 For the synthetic hurricane Florence and hurricane Irene, we saw an increased flooded area in comparison to FEMA  
311 (Table 4); for CI2, for example, the increase was almost 200% from IR1 to IR2. Again, this result confirms that  
312 accounting for river peak flow frequency alone does not effectively capture the severity of a flood hazard in the case  
313 of coastal locations.

314 For all the study sites for future Sandy, we saw consistent increases in flood extent (Table 4) from SD2 to SD4 and  
315 SD3 to SD5. Between SD2/SD3 and SD4/SD5, the only difference was the future projection of the flow. In comparison  
316 to the FEMA map, the percentage change ranged from -22.3 to +123.7. CI1, CI7, and CI8 for SD4 have less inundation  
317 than the FEMA 100-year map. This may be an indication of the significance of individual flood components specific

Formatted: Font color: Black

Formatted: Normal, Border: Top: (No border), Bottom: (No border), Left: (No border), Right: (No border), Between : (No border), Tab stops: 3.15", Centered + 6.3", Right

Formatted: Pattern: Clear, Highlight

Formatted: Pattern: Clear, Highlight

Formatted: Pattern: Clear, Highlight

Formatted: Font color: Black

Formatted: Normal, Border: Top: (No border), Bottom: (No border), Left: (No border), Right: (No border), Between : (No border), Tab stops: 3.13", Centered + 6.27", Right

318 to one site. For those sites, river flow might not be the most significant component of the flood. When we look at the  
319 hydrologic distances in table 1 CI1 and CI8 are closer to the coastline, making them more prone to coastal flooding  
320 than fluvial flooding. When we looked at SD5 (which added SLR), all the sites except CI8 showed more flooding than  
321 the FEMA 100-year flood map. Although CI8 had an increase of 22% in inundation compared to SD4.  
322 When we compare the worst-case future events (SD5 and IR2) to actual events (SD1 and IR1), we can see major  
323 changes in flood extents. The flood extent in all locations increased by about 60% on average for future Sandy with  
324 both SLR and coinciding tide (SD5) in comparison to the actual Sandy (SD1), with the highest impact in CI8 (+148%).  
325 Looking at Irene, the worst-case future scenario (IR2) increased the flood extent by about 30% on average for all  
326 locations compared to the actual event (IR2), with the highest impact in CI2 (101%). Among all the events, Florence  
327 had the lowest expected changes, between the current climate scenario (FL1) and the future one (FL2). One must note  
328 that hurricane Florence had no actual impact in the study area; the simulation for this event was based on a hurricane  
329 track forecast by GFS, which if materialized would have produced a flood inundation of almost 5 km<sup>2</sup> in CI3, and this  
330 extent could have increased by about 20% in the worst-case future scenario (FL2) that includes shifted tide and SLR.  
331 Five of the CIs were outside the FEMA 100-year flood zone, but they present flooding for FL1 and SD3. For FL2 all  
332 of the study sites were more vulnerable (positive % change), as compared to the FEMA map. Similar findings are  
333 presented for SD5, with the exception of except for CI8.

334

### 335 3.2 Flood depths over the domain

336 While flooding occurs in all the presented scenarios, both extent and depth vary greatly/significantly between the  
337 different simulations. Depth is important/critical to consider while preparing for risk management as it is used in  
338 determining flood damage.

339 The CDFs of water depth for the whole domain (Figure 8), confirm that the water depths derived for coupled events (  
340 i.e., high tide coinciding with surge peak, or SLR and future climate) are generally higher than those derived  
341 from events with independent drivers Note that for some cases (i.e. IR1 and IR2, for CI2 in Fig. 8) water  
342 depths increase very consistently as SLR increase. Large changes in the CDFs appears/appear for lower water  
343 depths. Thus, regions with generally lower hazard (depth), will likely experience/experience larger impacts under  
344 SLR. Results also confirm that scenarios with simultaneous high values for all these parameters implicated a higher  
345 vulnerability of the CIs. Comparing these changes in pairs [i.e. IR1 vs IR2, or SD1 vs SD3] also highlights that  
346 compound scenarios changes/change in the frequency of extreme values that go far beyond the average are much  
347 more pronounced than the related changes of the median depths (cumulative probability=0.50). In particular, it may  
348 be asserted that more expressed changes in extremes could lead to corresponding “hazard shift” for all CIs, as  
349 represented in Figure 8.

350

351 These results suggest that fluvial flow is not the only driver determining flood risk. Actual Irene (IR1) and synthetic  
352 Florence (FL) had higher river flood return periods than did actual Sandy (SD1) (Table 2). Nonetheless, the CDFs of  
353 the flood depth showed different behavior in terms of severity. For CI1, for example, IR1 had higher probabilities for

Formatted: Font color: Black

Formatted: Normal, Border: Top: (No border), Bottom: (No border), Left: (No border), Right: (No border), Between : (No border), Tab stops: 3.15", Centered + 6.3", Right

Formatted: Font color: Black

Formatted: Normal, Border: Top: (No border), Bottom: (No border), Left: (No border), Right: (No border), Between : (No border), Tab stops: 3.13", Centered + 6.27", Right

354 lower depth, followed by SD1 and FL1. In CI8, SD1 had higher probabilities for lower values of depth. These findings  
355 highlight that neither the severity of rainfall, nor the magnitude of river flow controls the flood characteristics, which  
356 are, rather, controlled by additional factors, such as storm surge, high tides, topography, and location of the site. CI7,  
357 for example, which is more coastal than the other CIs, presented increasing flood depth due to tidal timing.  
358 As expected, and as previously highlighted when considering the flood extent (Table 4), climate played an important  
359 role in flood hazard changes. Furthermore, the effect of SLR was also evident for all the events (IR, SD, and FL),  
360 increasing the flood depth for the same exceedance probability. For CI6, for example, the 50% exceedance  
361 corresponded to ~1 m depth of floodwater for IR1, increasing to ~1.5 m for IR2. For the CI4 and CI5 sites, for  
362 exceedance of 20%, actual Irene produced ~2 m of flood depth, whereas with SLR it was ~2.5 m. Another way to put  
363 it is that, for CI4/5, IR1 had an exceedance of ~20% for a flood depth of 2 m, whereas IR2 had an increased exceedance  
364 level of 40%. Similarly, for 50% exceedance, FL1 and FL2 corresponded to 1.5 m and 2 m depth of floodwater,  
365 respectively, and we saw the trend for the Sandy event scenarios (SD2–SD3; SD4–SD5) as well.  
366 This analysis highlighted that the timing of a storm is also crucial. The changes from SD1 to SD2 showed very well  
367 the impact of the shifted tide for all the sites. For CI3, for example, the 1 m flood depth had an exceedance of ~88%  
368 for SD2, whereas it was only ~23% for SD1.  
369 Analysis of the overall flood depth across the whole domain shows that the coincidence of fluvial flood, high tide, and  
370 storm surge results in a significant increase in flood risk. SD3 and SD5 had all the components of a compound flood  
371 and comparing them with SD1 gave us a clear idea of how severe a compound event can be in the future. CI3, for  
372 example, had exceedance levels of almost 30%, 85%, and 90%, respectively, for SD1, SD3, and SD5 for a flood depth  
373 of 1 m. This suggests the compound effect increases the intensity of the flood hazard.

### 374 3.3 Local risk for CI

375 Much of the flood damage in CI is incurred by components being submerged for a long period. Investigating the  
376 duration of the flood depth at the CI location (Figure 9) should be considered in planning for any protective measures,  
377 such as elevating or waterproofing equipment. If a critical infrastructure shows 0%, it means that for that  
378 scenario/event the water ~~didn't~~ did not reach the substation at all, at least during the simulated timeframe. This  
379 could be due to the water flooding other upstream locations, and therefore draining away from the station, or because  
380 the topography of the landscape actually prevented water from reaching the area for some specific events.  
381 According to our analysis, none of the scenarios has an actual impact on CI1. For the other CIs, comparing individual  
382 events we could see an increase in risk due to the compound hazard scenarios—that is, shifted tide and SLR. Important  
383 to note is that, for most of the sites, the compound risk due to SLR and tide timing was always higher for the lower  
384 water-level thresholds (0.5 m). This implies a higher risk for CI components currently positioned closer to the ground.  
385 Damage to the CI components is dictated by both the flood depth and the duration of submergence. The suggested  
386 high values of risk [increase percentage in inundation duration] (Figure 9) further imply differences in the timing of  
387 repairs. In the cases of CI7 and CI8 (Figure 9), the CIs remained submerged with 0.5 m of water for about 20% of the  
388 event period for actual Sandy, ~~but for~~ For the worst-case future Sandy scenario, the location was flooded for more

Formatted: Font color: Black

Formatted: Normal, Border: Top: (No border), Bottom: (No border), Left: (No border), Right: (No border), Between : (No border), Tab stops: 3.15", Centered + 6.3", Right

Formatted: Font color: Black

Formatted: Normal, Border: Top: (No border), Bottom: (No border), Left: (No border), Right: (No border), Between : (No border), Tab stops: 3.13", Centered + 6.27", Right

389 than 90% of the event duration. This demonstrates the increased flood risk to which future climate conditions expose  
390 CI.

391 Another ~~important~~critical insight was provided by the hurricane Florence scenarios. As mentioned earlier, Florence  
392 did not affect the study area, although an early GFS storm forecast track predicted landfall in Long Island and  
393 Connecticut. For this event, the estimated measure of risk was about 20%, and it was shown to increase to up to 40%  
394 for the lower water depth (0.5 m) threshold in some locations. The result of the simulated scenario allows for an  
395 assessment of potential damage and for an identification of equipment that might be affected by future events under  
396 current climatic conditions. In this regard, comparing the results for the different CIs during the Sandy scenarios  
397 revealed an interesting pattern. While we might have expected a ~~greater~~more significant impact over the whole domain  
398 when shifting the tide (Figure 9, Table. 3), we found different impacts in the CI locations. Notably, the risk appeared  
399 lower when the tides were shifted (Fig. 9) for some of the CIs (for example, CI5 and CI7). This can be explained by  
400 the fact that higher water levels in the domain were changing the water flows, allowing the flood to follow different  
401 drainable ways. This can be a very useful piece of information for deciding whether to and where to take measures in  
402 terms of flood occurrence and potentially relocating CIs to avoid catastrophic compound flood events.

403 From table 1 we can see that CI8 is the closest to the coastline followed by CI7, CI6, and CI5. From figure 9 we can  
404 see that all the CIs that are closer to the coastline are susceptible to changes in the downstream water level condition  
405 (Shifted tide/ SLR) (Table 3). CI4 is the farthest from the coast followed by CI3. Both the CIs show minimal response  
406 to changes in the coastal water level compared to CI5/ CI6/ CI7. This analysis gives us conclusive evidence of risk  
407 associated with the location of the CI from the coastline.

#### 408 4 Concluding Remarks

409 Preparing for the challenges posed by climate change requires ~~an~~ understanding of current actual, ~~-&~~ possible, and  
410 future scenario of tropical storm impacts, and a correct ~~understanding~~ interpretation of the hazard imposed by  
411 compound flooding. In this work we have developed and implemented a modeling framework that allows ~~to address~~  
412 ~~addressing~~ this task, focusing on coastal electric grid infrastructure (substations). To date, the design of these facilities  
413 typically has assumed the current climatic conditions. However, a changing climate, as well as ~~the~~ co-occurrence of  
414 compound drivers, and the resulting more extreme weather events mean those climate bands are becoming outdated,  
415 leaving infrastructure operating outside of its tolerance levels.

416 We explored a range of actual and synthetic hurricane scenarios, offering a system that could inform short- and long-  
417 term decisions. For the short-term decision, the framework allowed to investigate the characteristics of the hurricane-  
418 related inundation, considering the compound effect of riverine and coastal flooding coinciding, or not, with peak high  
419 tides. ~~Generally, hurricanes affect large areas, and the specific locations at which damage will occur are often difficult~~  
420 ~~to anticipate. Simulation of different scenarios can provide system operators with the ability to prepare for damage~~  
421 ~~and respond quickly once it has occurred—for example, by pre-positioning repair crews. Furthermore, by simulating~~  
422 ~~the impact using possible storm paths, the framework allows us to understand the potential impacts on the CI. The~~  
423 ~~framework proposed in this study evaluates the extent of flood nearby a critical coastal infrastructure caused by~~  
424 ~~possible extreme compound events. Each type of infrastructure system has specific elements vulnerable to specific~~

Formatted: Font color: Black

Formatted: Normal, Border: Top: (No border), Bottom: (No border), Left: (No border), Right: (No border), Between : (No border), Tab stops: 3.15", Centered + 6.3", Right

Formatted: Font color: Black

Formatted: Normal, Border: Top: (No border), Bottom: (No border), Left: (No border), Right: (No border), Between : (No border), Tab stops: 3.13", Centered + 6.27", Right

425 ~~water levels; we map those hazard infrastructure intersections where risks will be~~ allowed us to map those hazard-  
426 ~~infrastructure intersections where risks will be likely~~ exacerbated by climate change or compound events.

427 ~~The findings of this study can support flood mitigation; the FEMA 100-year map is used for designing infrastructure~~  
428 ~~and for making decisions on flood mitigation and flood insurance. Nonetheless, these maps must be updated because~~  
429 ~~flood risk is not static; changes in hydrology, topography, and land development all have an impact on flood~~  
430 ~~conditions.~~\_\_\_\_\_ The results show that the vulnerability of each substation is linked to the ~~different storms' event~~  
431 characteristics, and how they vary depending on the distance from the coast—that is, inland substations are less  
432 affected by surge and SLR and more affected by rainfall accumulation events (such as Irene). ~~The findings of this~~  
433 ~~study highlight that rising seas will allow storm surges to inundate areas farther inland and that flood hazard is likely~~  
434 ~~to grow as seas rise and storm surges become deeper. The results also highlight that tide surge SLR effects modeled~~  
435 ~~using only~~While coastal models in isolated open environments without considering fluvial effects on the flooding, or  
436 riverine models without appropriate downstream boundary conditions cannot capture the risk from tide surge SLR  
437 effects. ~~The variability in flood extent among scenarios implies that the modeling of individual flood drivers separately~~  
438 ~~can mischaracterize the true risk of flooding to coastal communities and critical infrastructure, introducing~~  
439 ~~uncertainties that make the design of long-lived infrastructure much~~ areas are more difficult. Significant losses can  
440 result in when the designs are inadequate and ill-adapted ~~vulnerable to CF, our analysis shows that significant impacts~~  
441 ~~due to climate~~ conditions change can be seen also inland, for increasing intensity of riverine events.

442 This study also ~~shows~~highlights that, for some locations, FEMA maps significantly underestimate the actual ~~storm~~  
443 ~~surge risk to structures near the shore relative to structures further inland, and it~~ flood risk, especially for CI in coastal  
444 areas. ~~These maps~~ generally ~~does not~~ fail to account for the impacts posed by simultaneous conditions, such as high  
445 tide and river flows, or for future climate impacts.

446 Future research should consider improved estimation methods, including more detailed information on the variability  
447 of river properties ( ~~i.e.~~, depth and width). Future works should also relate the frequency of inundation depths to  
448 return periods of precipitation, river flows, and surges, as well as differentiate among the individual effects of the  
449 components to determine the role of each in flooding impact. ~~This can be a very useful piece of information for~~  
450 ~~deciding whether and where to take measures in terms of flood occurrence and the potential relocation of CI to avoid~~  
451 ~~catastrophic compound flood events.~~

452 Notwithstanding these challenges, the findings of this study highlight that, whenever possible, risk assessments across  
453 different critical locations directly or indirectly affecting critical infrastructure should be based on a consistent set of  
454 compound risks. ~~The proposed analysis suggests planning and management strategies for critical infrastructure should~~  
455 ~~rely on historical flooding data, together with future storm scenarios and climate and SLR projections. The overall~~  
456 ~~impact on each critical structure in terms of flood extent and depth is unique.~~ This will ultimately allow the building  
457 of resilience into different components of critical infrastructure to enable the system to function even under disaster  
458 conditions or to recover more quickly.

459  
460 **Acknowledgments:** This work was supported by Eversource Energy.

**Formatted:** Font color: Black

**Formatted:** Normal, Border: Top: (No border), Bottom: (No border), Left: (No border), Right: (No border), Between : (No border), Tab stops: 3.15", Centered + 6.3", Right

**Formatted:** Font color: Black

**Formatted:** Normal, Border: Top: (No border), Bottom: (No border), Left: (No border), Right: (No border), Between : (No border), Tab stops: 3.13", Centered + 6.27", Right

461 **Author contributions:** MKh, GS, XS, EA conceived the study. XS and EA contributed to the conception of the  
462 hydrologic model. RL contributed to the production and analysis of the hydrologic model outputs. MKo and EN  
463 contributed to the analysis, and interpretation of the climatic data. MKh and GS contributed to the automation of the  
464 hydraulic model and the interpretation of its results. All authors participated in drafting the article and revising it  
465 critically for important intellectual content. All authors give the final approval of the published version.

466 **Competing interests.** The authors declare that they have no conflict of interest.  
467

## 468 References

469 Abi-Samra, N. and Henry, W.: Actions Before and After a Flood – Substation Protection and Recovery from Weather  
470 Related Water Damage, IEEE Power & Energy Magazine, pp. 52–58, Mar/Apr. 2011.

471 ~~Ahearn E.A., (2004). Scientific Investigations Report 2004-5160, <https://doi.org/10.3133/sir20045160>~~

472 ~~Barnard, P. L., Hoover, D., Hubbard, D. M., Snyder, A., Ludka, B. C., Allan, J., Kaminsky, G. M., Ruggiero, P.,  
473 Gallien, T. W., Gabel, L., McCandless, D., Weiner, H. M., Cohn, N., Anderson, D. L. and Serafin, K. A.: Extreme  
474 oceanographic forcing and coastal response due to the 2015–2016 El Niño, Nat. Commun., 8(1), 14365,  
475 doi:10.1038/ncomms14365, 2017.~~

476 Bevacqua, E., Maraun, D., Vousdoukas, M. I., Voukouvalas, E., Vrac, M., Mentaschi, L., Widmann, M.: Higher  
477 probability of compound flooding from precipitation and storm surge in Europe under anthropogenic climate change.  
478 Sci. Adv. 5, eaaw5531, 2019.

479 Blöschl, G., Hall, J., Parajka, J., Perdigão, R. A. P., Merz, B., Arheimer, B., Aronica, G. T., Bilibashi, A., Bonacci,  
480 O., Borga, M., Čanjevac, I., Castellarin, A., Chirico, G. B., Claps, P., Fiala, K., Frolova, N., Gorbachova, L., Gül, A.,  
481 Hannaford, J., Harrigan, S., Kireeva, M., Kiss, A., Kjeldsen, T. R., Kohnová, S., Koskela, J. J., Ledvinka, O.,  
482 Macdonald, N., Mavrova-Guirguinova, M., Mediero, L., Merz, R., Molnar, P., Montanari, A., Murphy, C., Osuch, M.,  
483 Ovcharuk, V., Radevski, I., Rogger, M., Salinas, J. L., Sauquet, E., Šraj, M., Szolgay, J., Viglione, A., Volpi, E.,  
484 Wilson, D., Zaimi, K. and Živković, N.: Changing climate shifts timing of European floods, Science (80-. ),  
485 357(6351), 588–590, doi:10.1126/science.aan2506, 2017.

486 ~~Bradbrook, K., Lane, S., Waller, S. and Bates, P.: Two-dimensional diffusion-wave modelling of flood inundation  
487 using a simplified channel representation, Int. J. River Basin Manag., 2, 211–223 [online] Available from:  
488 [https://research-information.bris.ac.uk/en/publications/two-dimensional-diffusion-wave-modelling-of-flood-](https://research-information.bris.ac.uk/en/publications/two-dimensional-diffusion-wave-modelling-of-flood-inundation-usin)  
489 [inundation-usin](https://research-information.bris.ac.uk/en/publications/two-dimensional-diffusion-wave-modelling-of-flood-inundation-usin) (Accessed 13 October 2020), 2004.~~

490 Cañizares, R., & Irish, J. L.: Simulation of storm-induced barrier island morphodynamics and flooding. Coastal  
491 Engineering, 55(12), 1089–1101. <https://doi.org/10.1016/J.COASTALENG.2008.04.006>, 2008.

492 Cariolet, J.-M.: Use of high water marks and eyewitness accounts to delineate flooded coastal areas: The case of Storm  
493 Johanna (10 March 2008) in Brittany, France. Ocean & Coastal Management, 53(11), 679–690.  
494 <https://doi.org/10.1016/J.OCECOAMAN.2010.09.002>, 2010.

Formatted: Font color: Black

Formatted: Normal, Border: Top: (No border), Bottom: (No border), Left: (No border), Right: (No border), Between : (No border), Tab stops: 3.15", Centered + 6.3", Right

Formatted: Font color: Black

Formatted: Normal, Border: Top: (No border), Bottom: (No border), Left: (No border), Right: (No border), Between : (No border), Tab stops: 3.13", Centered + 6.27", Right

495 Chang, S. E., McDaniels, T. L., Mikawoz, J., & Peterson, K.: Infrastructure failure interdependencies in extreme  
 496 events: power outage consequences in the 1998 Ice Storm. *Natural Hazards*, 41(2), 337–358.  
 497 <https://doi.org/10.1007/s11069-006-9039-4>, 2007.

498 Chou M.-D., and Suarez, M. J.: An efficient thermal infrared radiation parameterization for use in general circulation  
 499 models. *NASA Tech. Memo.* 104606, 3, 85pp, 1994.

500 Cook, A., Merwade, V., (2009).: Effect of topographic data, geometric configuration and modeling approach on  
 501 flood inundation mapping. *Journal of Hydrology*, 377, 1–2, 20, 131-142  
 502 <https://doi.org/10.1016/j.jhydrol.2009.08.015><https://doi.org/10.1016/j.jhydrol.2009.08.015>, 2009.

503 CtECO.: 2012 Impervious Surface Download,  
 504 [http://www.cteco.uconn.edu/projects/ms4/impervious](http://www.cteco.uconn.edu/projects/ms4/impervious2012.htm)  
 505 [2012.htm](http://www.cteco.uconn.edu/projects/ms4/impervious2012.htm), 2012.

506 CtECO: Connecticut Elevation (Lidar) Data, <http://www.cteco.uconn.edu/data/lidar/index.htm>, 2016.

507 D.A. Reed, M. D.A., Powell, M.D., and J.M. Westerman, J.M.: Energy Supply System Performance  
 508 for Hurricane Katrina. *Journal of Energy Engineering*, pp. 95–102, Dec. 2010.

509 Danielson, J.J. and Gesch, D.B.: Global multi-resolution terrain elevation data 2010 (GMTED2010) (p. 26). US  
 510 Department of the Interior, US Geological Survey, 20162011 .

511 Dawson, R. J., Thompson, D., Johns, D., Wood, R., Darch, G., Chapman, L., Hughes, P. N., Watson, G. V. R., Paulson,  
 512 K., Bell, S., Gosling, S. N., Powrie, W. and Hall, J. W.: A systems framework for national assessment of climate risks  
 513 to infrastructure, *Philos. Trans. R. Soc. A Math. Phys. Eng. Sci.*, 376(2121), doi:10.1098/rsta.2017.0298, 2018,  
 514 [Dazzi, S., Vacondio, R., & Mignosa, P.: Integration of a Levee Breach Erosion Model in a GPU-Accelerated 2D](https://doi.org/10.1029/2018WR023826)  
 515 [Shallow Water Equations Code. \*Water Resources Research\*, 55\(1\), 682-702. https://doi.org/10.1029/2018WR023826,](https://doi.org/10.1029/2018WR023826)  
 516 [2019.](https://doi.org/10.1029/2018WR023826)

517 de Bruijn, K. M., Maran, C., Zygnerski, M., Jurado, J., Burzel, A., Jeuken, C. and Obeysekera, J.: Flood resilience of  
 518 critical infrastructure: Approach and method applied to Fort Lauderdale, Florida, *Water (Switzerland)*, 11(3),  
 519 doi:10.3390/w11030517, 2019.

520 de Bruijn, K., Buurman, J., Mens, M., Dahm, R. and Klijn, F.: Resilience in practice: Five principles to enable societies  
 521 to cope with extreme weather events, *Environ. Sci. Policy*, 70, 21–30, doi:10.1016/j.envsci.2017.02.001, 2017.

522 Dee, D.P., Uppala, S.M., Simmons, A.J., Berrisford, P., Poli, P., Kobayashi, S., Andrae, U., Balmaseda, M.A.,  
 523 Balsamo, G., Bauer, P., Bechtold, P., Beljaars, A.C.M., van de Berg, L., Bidlot, J., Bormann, N., Delsol, C., Dragani,  
 524 R., Fuentes, M., Geer, A.J., Haimberger, L., Healy, S.B., Hersbach, H., Hólm, E.V., Isaksen, L., Kållberg, P., Köhler,  
 525 M., Matricardi, M., McNally, A.P., Monge-Sanz, B.M., Morcrette, J.-J., Park, B.-K., Peubey, C., de Rosnay, P.,  
 526 Tavolato, C., Thépaut, J.-N. and Vitart, F.: The ERA-Interim reanalysis: Configuration and performance of the data  
 527 assimilation system. *Quart. J. Roy. Meteor. Soc.*, 137, 553–597, doi: <https://doi.org/10.1002/qj.828>, 2011.

528 Dottori, F., Szewczyk, W., Ciscar, J. C., Zhao, F., Alfieri, L., Hirabayashi, Y., Bianchi, A., Mongelli, I., Frieler, K.,  
 529 Betts, R. A. and Feyen, L.: Increased human and economic losses from river flooding with anthropogenic warming,  
 530 *Nat. Clim. Chang.*, 8(9), 781–786, doi:10.1038/s41558-018-0257-z, 2018.

**Formatted:** Font color: Black

**Formatted:** Normal, Border: Top: (No border), Bottom: (No border), Left: (No border), Right: (No border), Between : (No border), Tab stops: 3.15", Centered + 6.3", Right

**Field Code Changed**

**Formatted:** Default Paragraph Font

**Formatted:** English (United Kingdom)

**Formatted:** English (United Kingdom)

**Formatted:** Font color: Black

**Formatted:** Normal, Border: Top: (No border), Bottom: (No border), Left: (No border), Right: (No border), Between : (No border), Tab stops: 3.13", Centered + 6.27", Right

531 FAO.: The digitized soil map of the world, World Soil Resource Rep. 67, FAO, Rome. FAO-UNESCO (1971–1981),  
532 Soil Map of the World (1:5,000,000), vol. 1–10, UNESCO, Paris, France. FAO-UNESCO (1974), Soil Map of the  
533 World (1:5,000,000), vol. 1 legend, UNESCO, Paris, France, 1991.

534 FEMA, CT DEEP (2013). Coastal Hazards Map Viewer Information  
535 <http://www.cteco.uconn.edu/viewers/coastalhazards.htm#surge>

536 FEMA.: Reducing Flood Effects in Critical Facilities. HSFE60-13-(April), 1–11, 2013.

537 Friedl M. A., Sulla-Menashe D., Tan B., Schneider A., Ramankutty N., Sibley A., & Huang X.: MODIS Collection 5  
538 global land cover: Algorithm refinements and characterization of new datasets. Remote Sensing of Environment,  
539 114(1), 168 10.1016/j.rse.2009.08.016–182), 2010.

540 Friedl, M., Sulla-Menashe, D.: MCD12Q1 MODIS/Terra+Aqua Land Cover Type Yearly L3 Global 500m SIN Grid  
541 V006. NASA EOSDIS Land Processes DAAC. <https://doi.org/10.5067/MODIS/MCD12Q1.006>, 2015.

542 ~~Gerald, A. M., Covey, C., Delworth, T., Latif, M., McAvaney, B., Mitchell, J. F. B., Stouffer, R. J., and Taylor, K.  
543 E. The WCRP-CMIP3 multimodel dataset: A new era in climate change research. Bulletin of American  
544 Meteorological Society, 2007.~~

545 Hallegatte, S., Green, C., Nicholls, R. J., Corfee-Morlot, J.: Future flood losses in major coastal cities. Nat Clim Chang  
546 3:802–806. doi: 10.1038/nclimate1979, 2013.

547 Hamman, J. J., Hamlet, A. F., Lee, S.-Y., Fuller, R. and Grossman, E. E.: Combined Effects of Projected Sea Level  
548 Rise, Storm Surge, and Peak River Flows on Water Levels in the Skagit Floodplain, Northwest Sci., 90(1), 57–78,  
549 doi:10.3955/046.090.0106, 2016.

550 ~~Hamman, J. J., Hamlet, A. F., Lee, S.-Y., Fuller, R., & Grossman, E. E.: Combined Effects of Projected Sea  
551 Level Rise, Storm Surge, and Peak River Flows on Water Levels in the Skagit Floodplain. Northwest Science,  
552 90(1), 57–78. <https://doi.org/10.3955/046.090.0106>, 2016.~~

553 Higgins, Wayne & Shi, Wei & Yarosh, E. & Joyce, R.W.: Climate Prediction Center (U.S.S.): Improved United States  
554 Precipitation Quality Control System [precipitation quality control system](#) and [Analysis; analysis](#). NCEP/Climate  
555 Prediction Center Atlas. 7., NOAA, National Weather Service, National Centers for Environmental  
556 Prediction, Climate Prediction Center: Camp Springs, MD, USA, 2000.

557 Hostache, R., Matgen, P., Schumann, G., Puech, C., Hoffmann, L., & Pfister, L.: Water Level Estimation and  
558 Reduction of Hydraulic Model Calibration Uncertainties Using Satellite SAR Images of Floods. IEEE Transactions  
559 on Geoscience and Remote Sensing, 47(2), 431–441. <https://doi.org/10.1109/TGRS.2008.2008718>, 2009.

560 Jordi, A., Georgas, N., Blumberg, A., Yin, L., Chen, Z., Wang, Y., Schulte, J., Ramaswamy, V., Runnels, D. and  
561 Saleh, F.: A next-generation coastal ocean operational system, Bull. Am. Meteorol. Soc., 100(1), 41–53,  
562 doi:10.1175/BAMS-D-17-0309.1, 2019.

563 Karagiannis, G.M., Chondrogiannis, S., Krausmann, E. and Turksezer, Z.I.: Power grid recovery after natural  
564 hazard impact. Science for Policy report by the Joint Research Centre (JRC), European Union.  
565 <https://doi.org/10.2760/87402>, 2017.

566 Koenig, T.A., Bruce, J.L., O'Connor, J.E., McGee, B.D., Holmes, R.R., Jr., Hollins, Ryan, Forbes, B.T., Kohn, M.S.,  
567 Schellekens, M.F., Martin, Z.W., and Pepler, M.C.: Identifying and preserving high-water mark data: U.S.S

Formatted: Font color: Black

Formatted: Normal, Border: Top: (No border), Bottom: (No border), Left: (No border), Right: (No border), Between : (No border), Tab stops: 3.15", Centered + 6.3", Right

Formatted: Font color: Black

Formatted: Normal, Border: Top: (No border), Bottom: (No border), Left: (No border), Right: (No border), Between : (No border), Tab stops: 3.13", Centered + 6.27", Right



568 Geological Survey Techniques and Methods, <https://doi.org/10.3133/t3A24>, 2016.  
569 Kwasinski, W.W. Weaver, P.L. Chapman and P.T. Krein, "Telecommunications Power Plant Damage Assessment for  
570 Hurricane Katrina – Site Survey and Follow-Up Results," IEEE Systems Journal, vol. 3, no. 3, pp. 277–287, Nov.  
571 2009.

572 Lackmann, G. M.: Hurricane Sandy before 1900, and after 2100. Bull. Amer. Meteor. Soc., 96, 547-560, doi:  
573 10.1175/BAMS-D-14-00123.1, 2015.

574 Leonard, M., Westra, S., Phatak, A., Lambert, M., Van Den Hurk, B., McInnes, K., ... Stafford-Smith, M.: A  
575 compound event framework for understanding extreme impacts. WIREs Clim Change, 5, 113–128.  
576 <https://doi.org/10.1002/wcc.252>, 2014.

577 Lin, N., Kopp, R. E., Horton, B. P., & Donnelly, J. P.: Hurricane Sandy's flood frequency increasing from year 1800  
578 to 2100. Proceedings of the National Academy of Sciences of the United States of America, 113(43), 12071–12075.  
579 <https://doi.org/10.1073/pnas.1604386113>, 2016.

580 Marsooli, R., Lin, N., Emanuel, K., & Feng, K.: Climate change exacerbates hurricane flood hazards along US  
581 Atlantic and Gulf Coasts in spatially varying patterns. Nature Communications, 10(1).  
582 <https://doi.org/10.1038/s41467-019-11755-z>, 2019.

583 McEvoy, D., Ahmed, I., Mullett, J.: The impact of the 2009 heat wave on Melbourne's critical infrastructure. Local  
584 Environ 17:783–796. doi: 10.1080/13549839.2012.678320, 2012.

585 Meehl, G. A., Covey, C., Taylor, K. E., Delworth, R. J., Stouffer, M. T., Latif, B. M., McAvaney, J. F., B.,  
586 Mitchell, J. F. B., Stouffer, R. J., and Taylor, K. E.: The WCRP CMIP3 multimodel dataset: A new era in  
587 climate climatic change research. Bull. Amer. Meteor. Soc., 88(9), 1383–1394, doi:10.1175/BAMS-88-  
588 9-1383, 2007.

589 Mlawer, E. J., Taubman, S. J., Brown, P. D., Iacono, M. J. and Clough, S. A.: Radiative transfer for inhomogeneous  
590 atmospheres: RRTM, a validated correlated-k model for the longwave. J. Geophys. Res., 102, 16663–16682.  
591 doi:10.1029/97JD00237, 1997.

592 Moftakhari, H. R., Salvadori, G., AghaKouchak, A., Sanders, B. F., & Matthew, R. A.: Compounding effects of sea  
593 level rise and fluvial flooding. Proceedings of the National Academy of Sciences of the United States of America,  
594 114(37), 9785–9790. <https://doi.org/10.1073/pnas.1620325114>, 2017.

595 Muis, S., Verlaan, M., Winsemius, H. C., Aerts, J. C. J. H. and Ward, P. J.: A global reanalysis of storm surges and  
596 extreme sea levels, Nat. Commun., 7, doi:10.1038/ncomms11969, 2016.

597 NOAA.: NOAA's STATE OF THE COAST: National Coastal Population Report, 2013.

598 O'Donnell, J.: Sea Level Rise Connecticut Final Report. [https://circa.uconn.edu/wp-](https://circa.uconn.edu/wp-content/uploads/sites/1618/2019/02/SeaLevelRiseConnecticut-Final-Report.pdf)  
599 [content/uploads/sites/1618/2019/02/SeaLevelRiseConnecticut-Final-Report.pdf](https://circa.uconn.edu/wp-content/uploads/sites/1618/2019/02/SeaLevelRiseConnecticut-Final-Report.pdf), 2017. (last accessed January 10,  
600 2020)

601 Pant, R., Thacker, S., Hall, J. W., Alderson, D. and Barr, S.: Critical infrastructure impact assessment due to flood  
602 exposure, J. Flood Risk Manag., 11(1), 22–33, doi:10.1111/jfr3.12288, 2018.

Formatted: Font color: Black

Formatted: Normal, Border: Top: (No border), Bottom: (No border), Left: (No border), Right: (No border), Between : (No border), Tab stops: 3.15", Centered + 6.3", Right

Formatted: Font color: Black

Formatted: Normal, Border: Top: (No border), Bottom: (No border), Left: (No border), Right: (No border), Between : (No border), Tab stops: 3.13", Centered + 6.27", Right

603 Pasquier, U., He, Y., Hooton, S., Goulden, M. and Hiscock, K. M.: An integrated 1D–2D hydraulic modelling  
604 approach to assess the sensitivity of a coastal region to compound flooding hazard under climate change, *Nat. Hazards*,  
605 98(3), 915–937, doi:10.1007/s11069-018-3462-1, 2019.

606 Pearson, J., Punzo, G., Mayfield, M., Brighty, G., Parsons, A., Collins, P., Jeavons, S. and Tagg, A.: Flood resilience:  
607 consolidating knowledge between and within critical infrastructure sectors, *Environ. Syst. Decis.*, 38(3), 318–329,  
608 doi:10.1007/s10669-018-9709-2, 2018.

609 Powers, J. G., Klemp, J. B., Skamarock, W. C., Davis, C. A., Dudhia, J., Gill, D. O., Coen, J. L. and Gochis, D. J.:  
610 The Weather Research and Forecasting Model: Overview, system efforts, and future directions. *Bull. Amer.*  
611 *Meteor. Soc.*, 98, 1717–1737, <https://doi.org/10.1175/BAMS-D-15-00308.1>, 2017.

612 Quinn, N., Bates, P. D., Neal, J., Smith, A., Wing, O., Sampson, C., Smith, J. and Heffernan, J.: The Spatial  
613 Dependence of Flood Hazard and Risk in the United States, *Water Resour. Res.*, 55(3), 1890–1911,  
614 doi:10.1029/2018WR024205, 2019.

615 Schumann, G., Hostache, R., Puech, C., Hoffmann, L., Matgen, P., Pappenberger, F., & Pfister, L.: High-Resolution  
616 3-D Flood Information From Radar Imagery for Flood Hazard Management. *IEEE Transactions on Geoscience and*  
617 *Remote Sensing*, 45(6), 1715–1725. <https://doi.org/10.1109/TGRS.2006.888103>, 2007a.

618 Schumann, G., Matgen, P., Cutler, M. E. J., Black, A., Hoffmann, L., & Pfister, L.: Comparison of remotely sensed  
619 water stages from LiDAR, topographic contours and SRTM. *ISPRS Journal of Photogrammetry and Remote Sensing*,  
620 63(3), 283–296. <https://doi.org/10.1016/j.isprsjprs.2007.09.004>, 2008.

621 Schumann, G., Matgen, P., Hoffmann, L., Hostache, R., Pappenberger, F., & Pfister, L.: Deriving distributed  
622 roughness values from satellite radar data for flood inundation modelling. *Journal of Hydrology*, 344(1–2), 96–111.  
623 <https://doi.org/10.1016/j.jhydrol.2007.06.024>, 2007b.

624 Shen, X., & Anagnostou, E. N.: A framework to improve hyper-resolution hydrological simulation in snow-affected  
625 regions. *Journal of Hydrology*, 552, 1–12. <https://doi.org/10.1016/j.jhydrol.2017.05.048>, 2017.

626 Skamarock, W. C., Klemp, J. B., Dudhia, J., Gill, D. O., Barker, D. M., Duda, M. G., Huang, X., Wang, W. and  
627 Powers, J. G.: A description of the Advanced Research WRF version 3. NCAR Tech. Note NCAR/TN-475+STR,  
628 113 pp., <https://doi.org/10.5065/D68S4MVH>, 2008.

629 Song–You, H., Noh, Y. and Dudhia, J.: A new vertical diffusion package with an explicit treatment of  
630 entrainment processes. *Mon. Wea. Rev.*, 134, 2318–2341. doi:10.1175/MWR3199.1, 2006.

631 Székely, G. J., Rizzo, M. L. and Bakirov, N. K.: MEASURING AND TESTING DEPENDENCE BY  
632 CORRELATION OF DISTANCES, *Ann. Stat.*, 35(6), 2769–2794, doi:10.1214/009053607000000505, 2007.

633 Tewari, M.F., Chen, W., Wang, J., Dudhia, M.A., LeMone, K., Mitchell, M.E., Gayno, G., Wegiel, J. and Cuenca,  
634 R.H.: Implementation and verification of the unified NOAA land surface model in the WRF model. 20th  
635 conference on weather analysis and forecasting/16th conference on numerical weather prediction, pp. 11–15, 2004.

636 Thompson, G., Paul, R. F., Roy, M. R. & William, D. H.: Explicit Forecasts of Winter Precipitation Using an  
637 Improved Bulk Microphysics Scheme. Part II: Implementation of a New Snow Parameterization. *Mon. Wea.*  
638 *Rev.*, 136, 5095–5115. doi:10.1175/2008MWR2387.1, 2008.

639 [U.S.S](#)

Formatted: Font color: Black

Formatted: Normal, Border: Top: (No border), Bottom: (No border), Left: (No border), Right: (No border), Between : (No border), Tab stops: 3.15", Centered + 6.3", Right

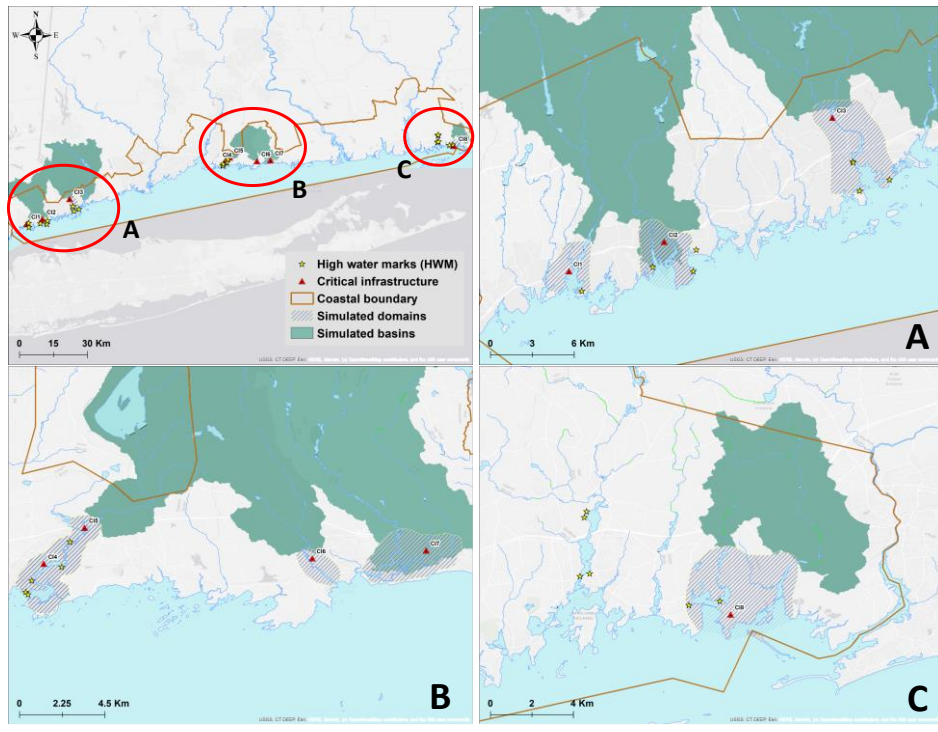
Formatted: Font color: Black

Formatted: Normal, Border: Top: (No border), Bottom: (No border), Left: (No border), Right: (No border), Between : (No border), Tab stops: 3.13", Centered + 6.27", Right

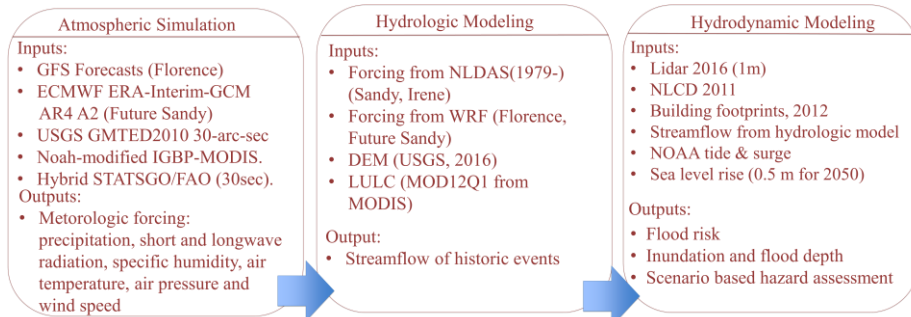
640 [Viero, D. P., D'Alpaos, A., Carniello, L., & Defina, A.: Mathematical modeling of flooding due to river bank failure.](#)  
641 [Advances in Water Resources, 59, 82-94. <https://doi.org/10.1016/j.advwatres.2013.05.011>, 2013.](#)  
642 [Viero, D. P., Roder, G., Matticchio, B., Defina, A., & Tarolli, P.: Floods, landscape modifications and population](#)  
643 [dynamics in anthropogenic coastal lowlands: The Polesine \(northern Italy\) case study. \*Science of The Total\*](#)  
644 [Environment, 651, 1435-1450. <https://doi.org/10.1016/j.scitotenv.2018.09.121>, 2019.](#)  
645 [Vousdoukas, M. I., Mentaschi, L., Voukouvalas, E., Verlaan, M., Jevrejeva, S., Jackson, L. P. and Feyen, L.: Global](#)  
646 [probabilistic projections of extreme sea levels show intensification of coastal flood hazard, \*Nat. Commun.\*, 9\(1\), 1–](#)  
647 [12, doi:10.1038/s41467-018-04692-w, 2018.](#)  
648 [Vousdoukas, M. I., Mentaschi, L., Voukouvalas, E., Verlaan, M., Jevrejeva, S., Jackson, L. P. and Feyen, L.: Global](#)  
649 [probabilistic projections of extreme sea levels show intensification of coastal flood hazard, \*Nat. Commun.\*, 9\(1\), 1–](#)  
650 [12, doi:10.1038/s41467-018-04692-w, 2018.](#)  
651 [Wahl, T., Ward, P., Winsemius, H., AghaKouchak, A., Bender, J., Haigh, I., ... Westra, S.: When Environmental](#)  
652 [Forces Collide. \*Eos\*, 99. <https://doi.org/10.1029/2018EO099745>, 2018.](#)  
653 [Warner, N. N., & Tissot, P. E.: Storm flooding sensitivity to sea level rise for Galveston Bay, Texas. \*Ocean\*](#)  
654 [Engineering, 44, 23–32. <https://doi.org/10.1016/J.OCEANENG.2012.01.011>, 2012.](#)  
655 [Winsemius, H. C., Van Beek, L. P. H., Jongman, B., Ward, P. J. and Bouwman, A.: A framework for global river](#)  
656 [flood risk assessments, \*Hydrol. Earth Syst. Sci.\*, 17, 1871–1892, doi:10.5194/hess-17-1871-2013, 2013.](#)  
657 [Xia, Y., Mitchell, K., Ek, M., Sheffield, J., Cosgrove, B., Wood, E., ... Mocko, D. .: Continental-scale water and](#)  
658 [energy flux analysis and validation for the North American Land Data Assimilation System project phase 2 \(NLDAS-](#)  
659 [2\): 1. Intercomparison and application of model products. \*Journal of Geophysical Research: Atmospheres\*, 117\(D3\),](#)  
660 [n/a-n/a. <https://doi.org/10.1029/2011JD016048>, 2012.](#)  
661 [Xian, S., Lin, N. and Hatzikyriakou, A.: Storm surge damage to residential areas: a quantitative analysis for Hurricane](#)  
662 [Sandy in comparison with FEMA flood map, \*Nat. Hazards\*, 79\(3\), 1867–1888, doi:10.1007/s11069-015-1937-x, 2015.](#)  
663 [Ziervogel, G., New, M., Archer van Garderen, E., Midgley, G., Taylor, A., Hamann, R., Stuart-Hill, S., Myers, J. and](#)  
664 [Warburton, M.: Climate change impacts and adaptation in South Africa. \*Wiley Interdiscip Rev Clim Chang\* 5:605–](#)  
665 [620. <https://doi.org/10.1002/wcc.295> , 2014.](#)  
666 [Zeng, N., Adams, C., Clark, H., ... Westra, S.: Climate change impacts on South African hydrology. \*Rev Clim Chang\*, 6\(5\), 611-624, 2014.](#)  
667 [Future climate risk from compound events. \*Nature Climate Change\*, 8\(6\), 469–477. \[https://doi.org/10.1038/s41558-\]\(https://doi.org/10.1038/s41558-018-0156-3\)](#)  
668 [018-0156-3, 2018.](#)  
669  
670

**Formatted:** Font color: Black  
**Formatted:** Normal, Border: Top: (No border), Bottom: (No border), Left: (No border), Right: (No border), Between : (No border), Tab stops: 3.15", Centered + 6.3", Right

**Formatted:** Font color: Black  
**Formatted:** Normal, Border: Top: (No border), Bottom: (No border), Left: (No border), Right: (No border), Between : (No border), Tab stops: 3.13", Centered + 6.27", Right



671  
 672 **Figure 1:** Study area with associated watersheds and simulation domains. Locations of substations and USGS high water  
 673 marks are also shown. Red circles in the top left-hand panel, and marked with A, B, and C are highlighted in the panels A  
 674 to C respectively. Background map by ESRI web-services, provided by UConn/CTDEEP, Esri, Garmin, USGS, NGA,  
 675 EPA, USDA, NPS



676  
 677 **Figure 2:** Considered framework including atmospheric simulations, hydrologic, and hydrodynamic modeling. Hurricane  
 678 events (actual and simulated), and inputs and outputs of each component are shown. Readers should refer to chapter 2.2  
 679 for specifications

**Formatted:** Font color: Black

**Formatted:** Normal, Border: Top: (No border), Bottom: (No border), Left: (No border), Right: (No border), Between : (No border), Tab stops: 3.15", Centered + 6.3", Right

**Formatted:** Font color: Black

**Formatted:** Normal, Border: Top: (No border), Bottom: (No border), Left: (No border), Right: (No border), Between : (No border), Tab stops: 3.13", Centered + 6.27", Right

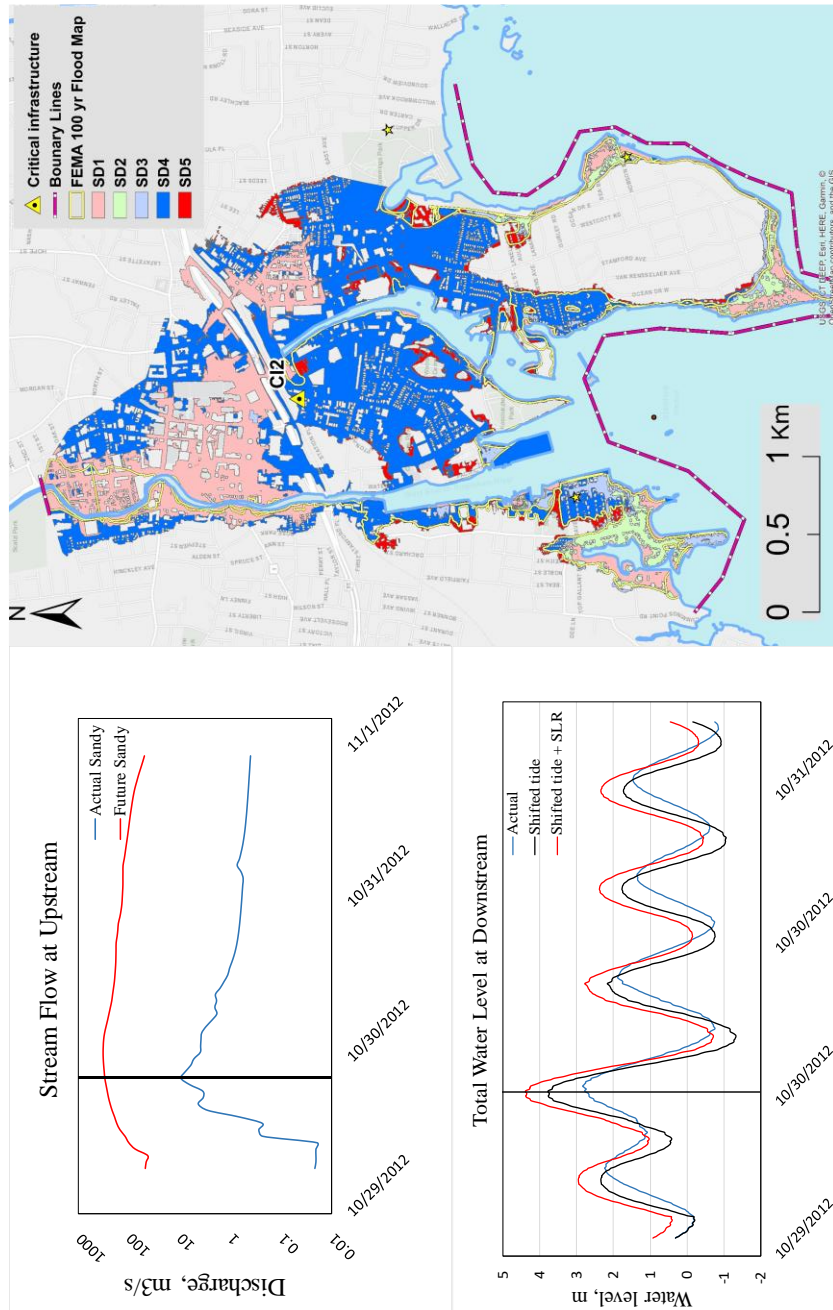


Figure 3- Example of different scenarios showing the upstream boundary condition (top left-hand panel, including the discharge for actual Sandy and future Sandy), and downstream boundary (bottom left-hand panel, including tide, shifted tide, and shifted tide with SLR). Output flood extent is also shown (right-hand panel), including results for SD1 to SD5 (reader should refer to Tab. 3 and chapter 2.2 for specification on the scenarios). Background map on the right-hand panel by ESRI web-services, provided by UConn/CFDEEP, Esri, Garmin, USGS, NGA, EPA, USDA, NPS

Figure 3: Example of different scenarios showing the upstream boundary condition (top left-hand panel, including the discharge for actual Sandy and future Sandy), and downstream boundary (bottom left-hand panel, including tide, shifted tide, and shifted tide with SLR). Output flood extent is also shown (right-hand panel), including results for SD1 to SD5 (reader should refer to Tab. 3 and chapter 2.2 for specification on the scenarios). Background map on the right-hand panel by ESRI web-services, provided by UConn/CTDEEP, Esri, Garmin, USGS, NGA, EPA, USDA, NPS

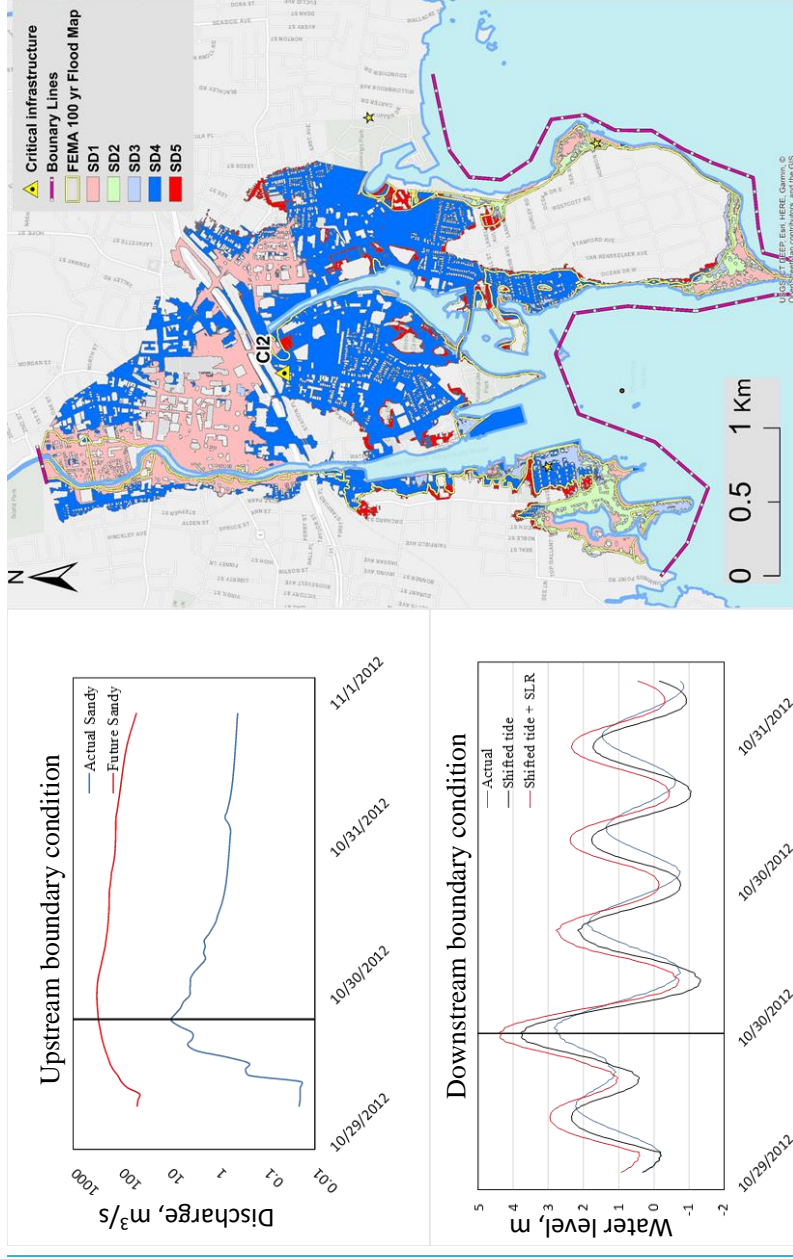


Figure 3: Example of different scenarios showing the upstream boundary condition (top left-hand panel, including the discharge for actual Sandy and future Sandy), and downstream boundary (bottom left-hand panel, including tide, shifted tide, and shifted tide with SLR). Output flood extent is also shown (right-hand panel), including results for SD1 to SD5 (reader should refer to Tab. 3 and chapter 2.2 for specification on the scenarios). Background map on the right-hand panel by ESRI web-services, provided by UConn/CTDEEP, Esri, Garmin, USGS, NGA, EPA, USDA, NPS

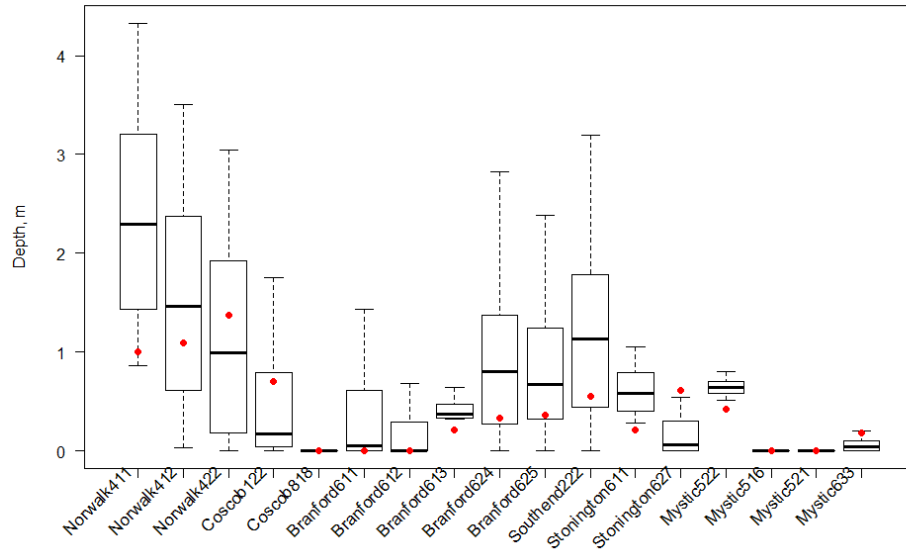


Figure 4: Validation results (boxplot of water depth within 10x10m around the high-water mark -HWM- location) compared to selected HWM (red dots) by USGS



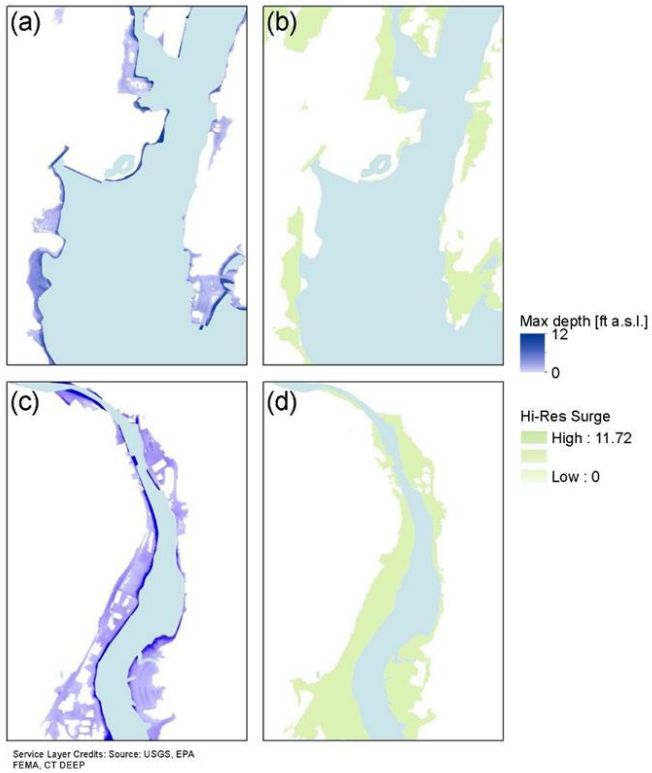


Figure 5: Comparison between the results of the proposed model for two selected locations (a,c, CI<sub>1</sub> and CI<sub>2</sub> respectively) and the maximum surge extent as proposed by CI Eco (c,d respectively).

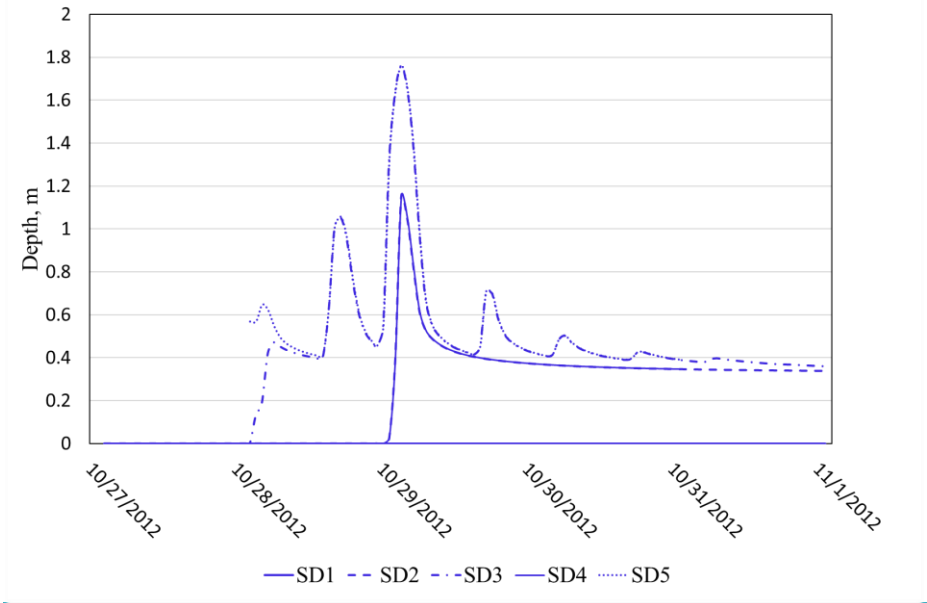


Figure 6: Example of time series of depth values for the different scenarios of Sandy event at CI3 [SD1 to SD5, readers should refer to Table 3 and chapter 2.4 for specification on the scenarios]

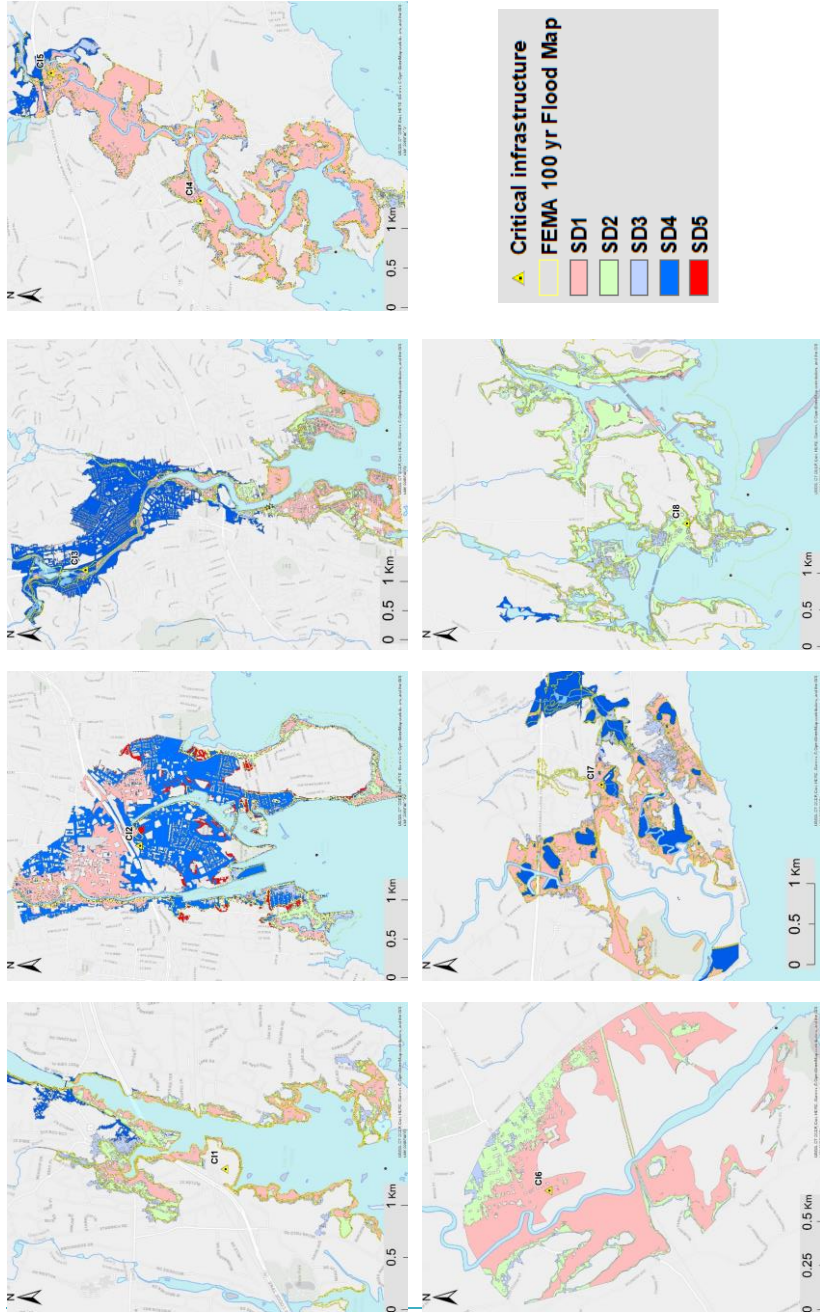


Figure 7a: Map overlay of maximum inundation for all the study domains containing CH through CH8 for the scenarios of Sandy [SD1 to SD5, readers should refer to Table 3 and chapter 2.2 for specification on the scenarios]

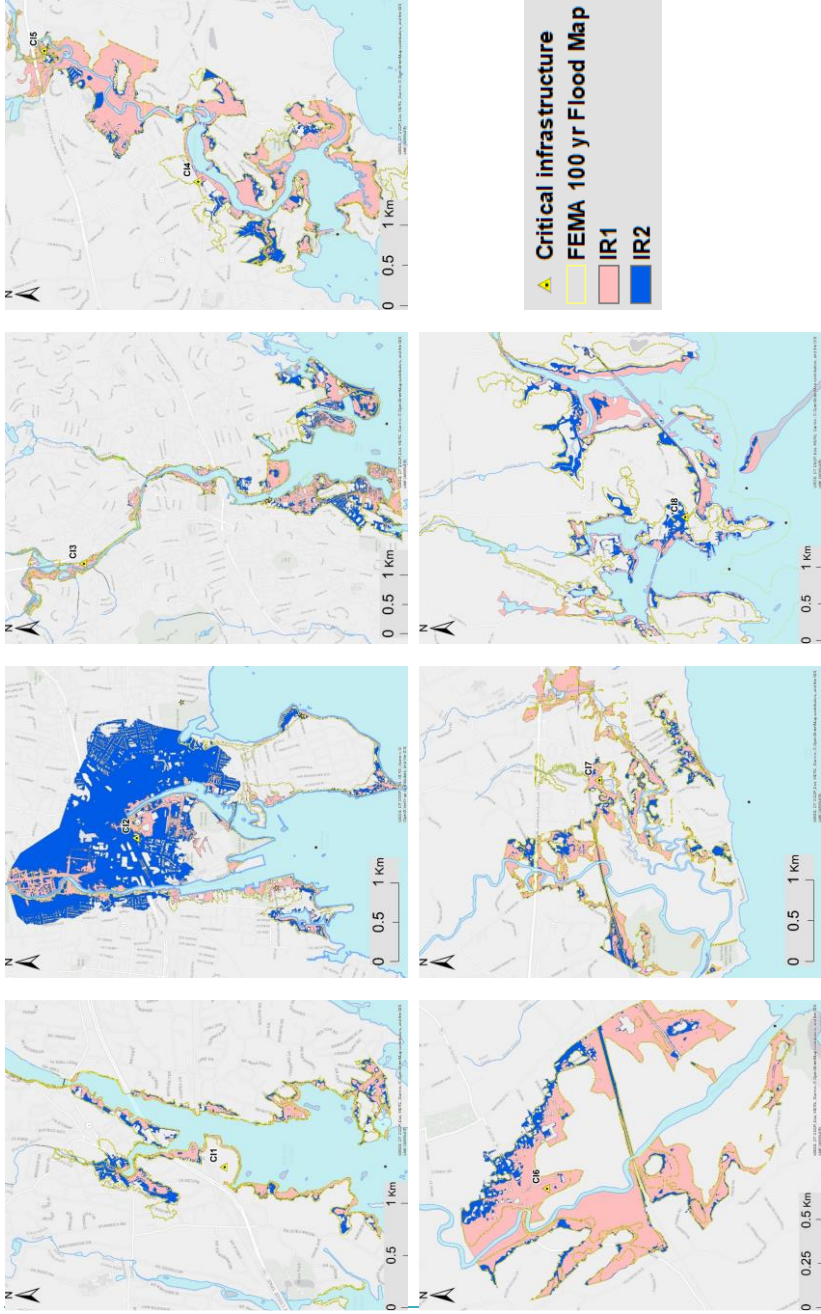


Figure 7a: Map overlay of maximum inundation for all the study domains containing CII through CI8 for the scenarios of Sandy [SD1 to SD5, readers should refer to Table 3 and chapter 2.2 for specification on the scenarios]

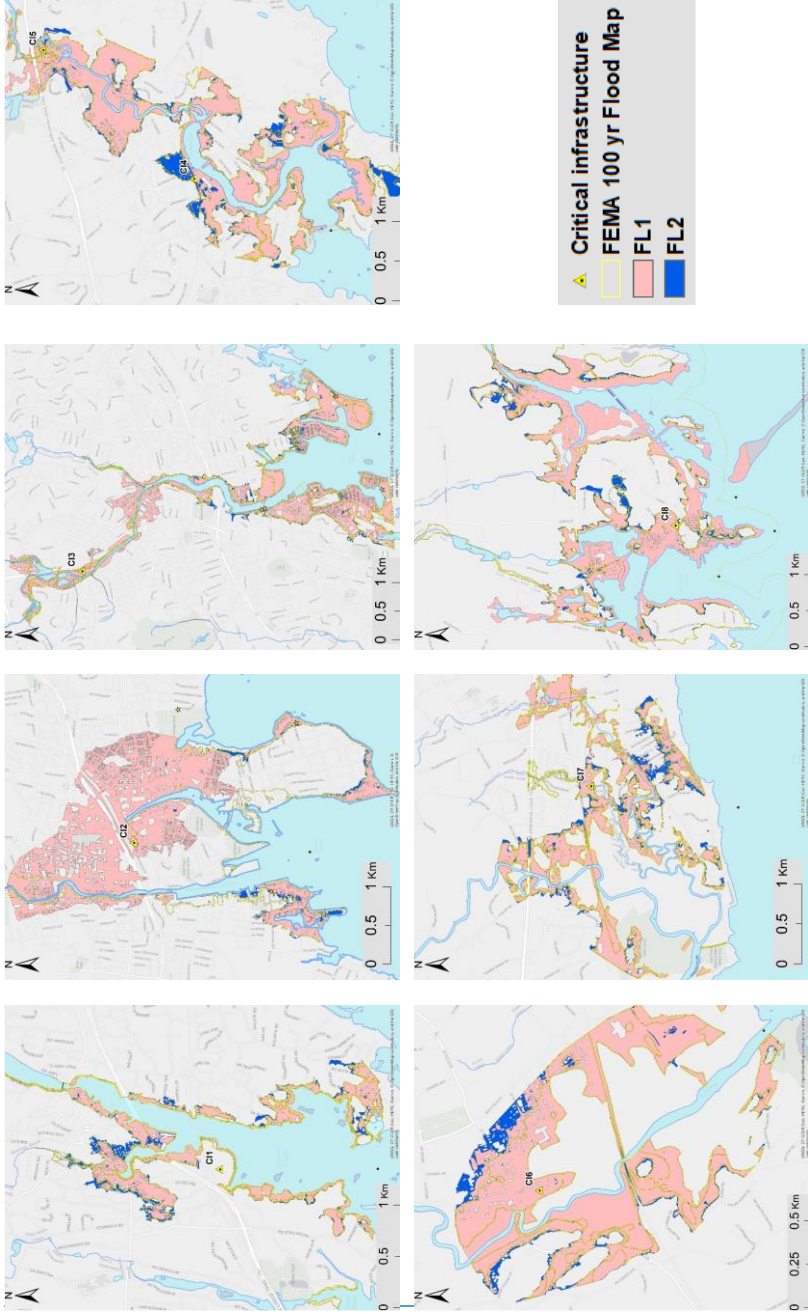


Figure 7a: Map overlay of maximum inundation for all the study domains containing CII through C18 for the scenarios of Sandy [SD1 to SD5, readers should refer to Table 3 and chapter 2.2 for specification on the scenarios]

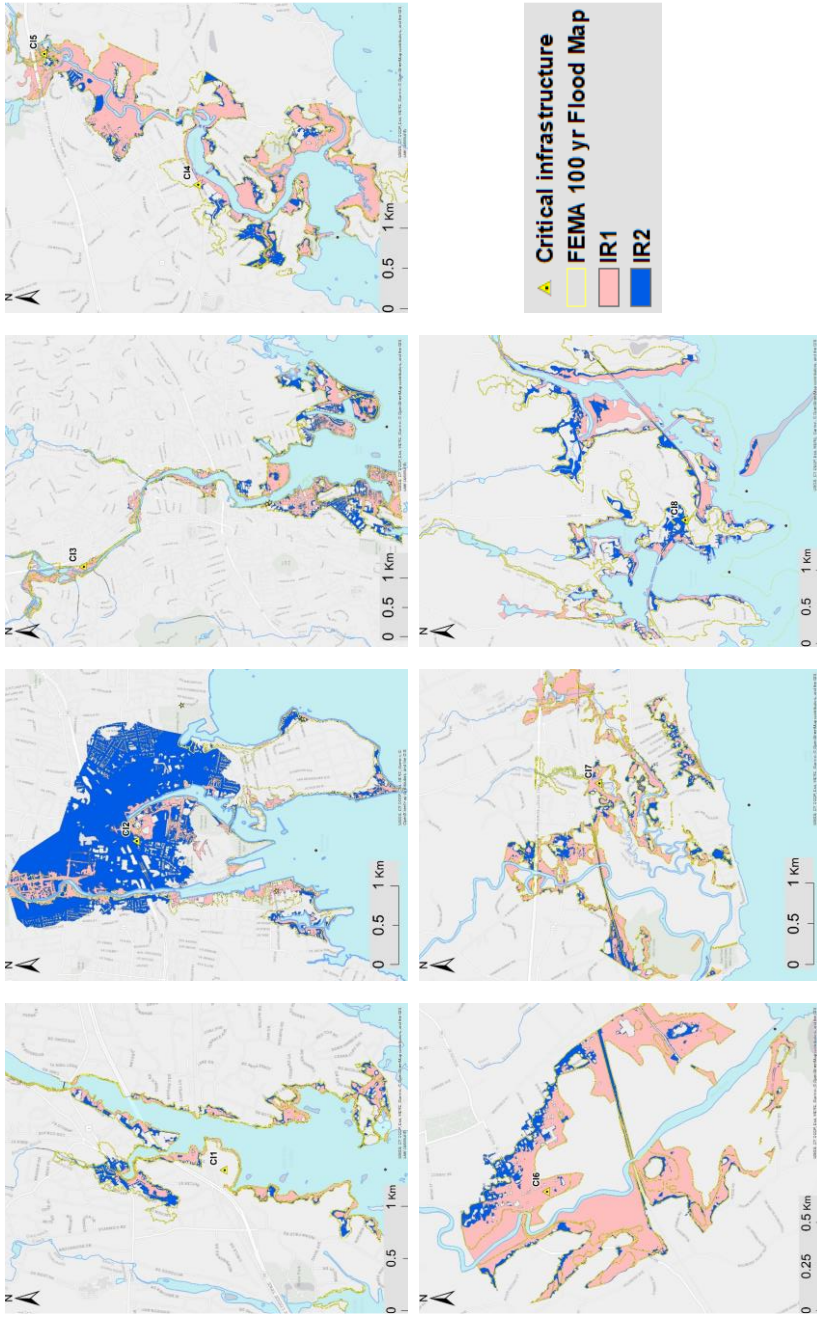


Figure 7b: Map overlay of maximum inundation for all the study domains containing CH1 through CH8 for the scenarios of Irene [IR1 and IR2, readers should refer to Tab. 3 and chapter 2.2 for specification on the scenarios]. Background map by ESRI web-services, provided by UConn/CTDEEP, Estri, Garmin, USGS, NGA, EPA, USDA, NPS.

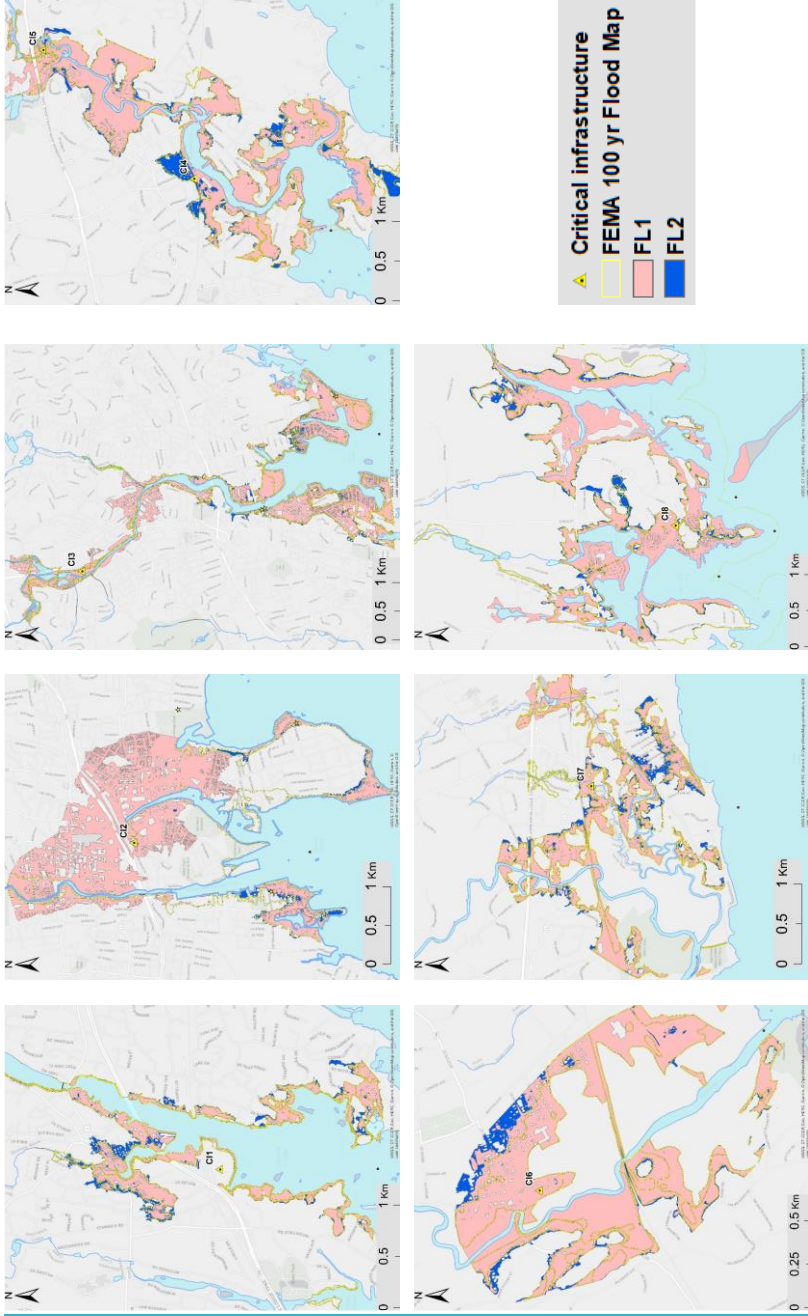


Figure 7c: Map overlay of maximum inundation for all the study domains containing CI through C18 for the scenarios of Florence [FL1 and FL2, readers should refer to Table 3 and chapter 2.2 for specification on the scenarios]. Background map by ESRI web-services, provided by UConn/CTDEEP, Esri, Garmin, USGS, NGA, EPA, USDA, NPS

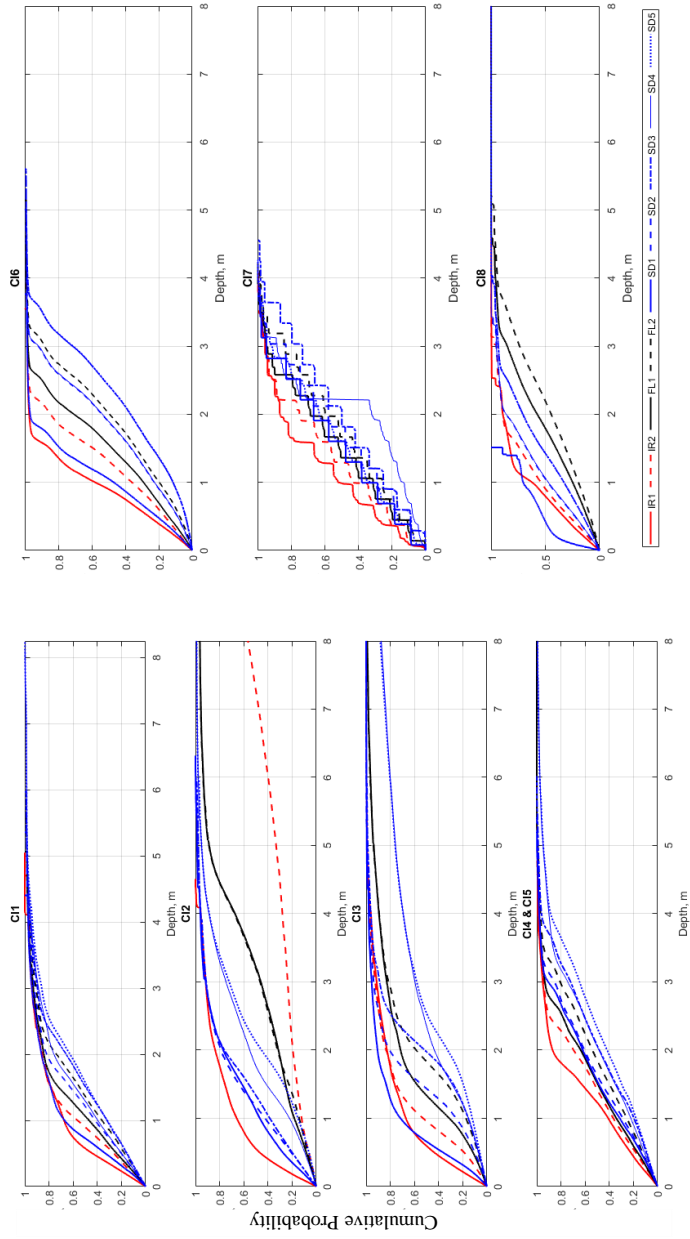
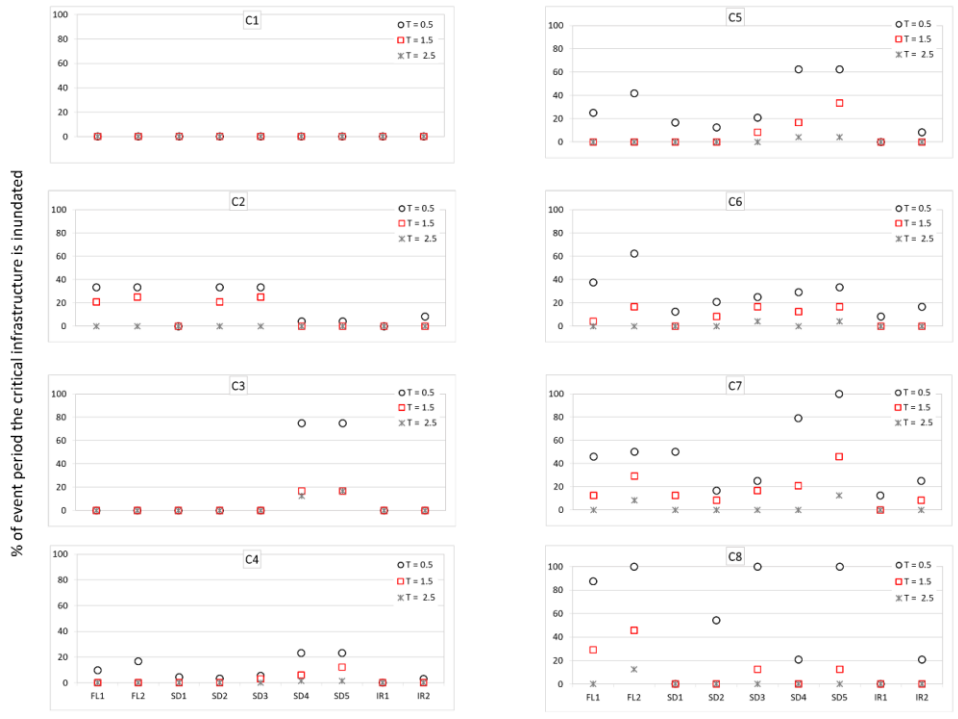


Figure 8: Cumulative density plot of the depth of all the flooded cells during maximum inundation. Hurricanes scenarios are labelled according to Table 3 and explained in chapter 2.2. Critical infrastructures are labelled C11 to C18, as described in Table 1.





Formatted

Figure 9: Peak over threshold ( $T=0.5, 1.5,$  and  $2.5m$ ) at selected critical infrastructures. Hurricanes scenarios, along the x-axis, are labeled according to Table 3 and explained in chapter 2.2. Critical infrastructures are labeled C11 to C18, as described in Table 1.

Formatted: Font: 9 pt, Bold

Formatted: Font: 9 pt, Bold

Formatted: Normal, Space After: 10 pt

**Table 1-1: Study area- Characteristics of the considered CIs, with river and model domain information. Basin area represents the area of the underlining watershed; domain area is the extent of the simulation domain; reach length represents the length of the stream within the domain; hydrologic distance represents the distance from each CI to the coastline.**

Critical Infrastructure (CI)	Town	Rivers	Basin area, km <sup>2</sup>	Domain area, km <sup>2</sup>	Reach length, km	Hydrologic distance, km
CI1	Coscob	Mianus River	216.6	7.5	7.8	4.5
CI2	Southend	Rippowam River	308.4	12.1	4.9	5.3
CI3	Norwalk	Norwalk River	268.7	20.7	8.3	7.8
CI4/ CI5	Branford	Branford River	84.5	7.9	6.7	8.8/5.3
CI6	Guilford	West River	126.4	2.2	3.7	5.1
CI7	Madison	East & Neck Rivers	173.0	8	5.3	6.8
CI8	Stonington	Stonington harbor	10.0	14.9	5.2	2.9

**Formatted:** Font: 9 pt, Bold, Font color: Black

**Formatted:** Font: 9 pt, Bold, Font color: Black

**Formatted:** Font color: Black

**Table 2: Model domain information for Florence**

Horizontal Resolution	18, 6, and 2 km
Vertical levels	28
Horizontal Grid Scheme	Arakawa C grid
Nesting	Two-way nesting
Convective parameterization	Grell 3D ensemble scheme (18 and 6 km grids only)
Microphysics option	Thompson graupel scheme (Thompson et al., 2008)
Longwave Radiation option	RRTM scheme (Mlawer et al., 1997)
Shortwave Radiation option	Goddard Shortwave scheme (Chou and Suarez 1994)
Surface-Layer option	Monin-Obukhov Similarity scheme
Land-Surface option	Noah Land-Surface Model (Tewari et al., 2004)
Planetary Boundary Layer	Yonsei scheme (Song-You et al., 2006)

**Formatted:** Font: 9 pt, Bold, Font color: Black

**Formatted:** Normal, Space After: 10 pt, Border: Top: (No border), Bottom: (No border), Left: (No border), Right: (No border), Between : (No border)

**Formatted:** Font color: Black

**Formatted:** Font: 10 pt

**Formatted:** Font: 10 pt

**Formatted Table**

**Formatted:** Font: 10 pt

**Formatted:** Font: 10 pt

**Formatted:** Font: 10 pt

**Formatted:** Font: 10 pt

**Formatted:** Font: 10 pt

**Formatted:** English (United Kingdom)

**Formatted:** Font: 10 pt, English (United Kingdom)

**Formatted:** Font: 10 pt

**Formatted:** Font: 10 pt

**Formatted:** Font: 10 pt

**Formatted:** Font: 10 pt

**Formatted:** English (United Kingdom)

**Formatted:** Font: 10 pt, English (United Kingdom)

**Formatted:** Font: 10 pt

**Table 3: Peak Tide, Surge at the maximum total water level instance, Accumulated precipitation & peak flows (with return period reported within brackets) for the simulated scenarios. Reader— The reader should refer to Chapter 2.2 for a detailed description of each hurricane scenario (IR for Irene, SD for Sandy, FL for Florence). The “\*\*” denotes the scenarios having sea level rise (SLR) added to the surge. Critical infrastructures are labelled CI1 to CI8 according to Table 1.**

Scenarios		CI1	CI2	CI3	CI4/ CI5	CI6	CI7	CI8
FL1	Tide (m)	0.99	0.99	0.99	0.94	0.94	0.94	0.17
	Surge (m)	2.51	2.51	2.51	2.56	2.46	2.56	3.33
	Accumulated precipitation (mm)	128.5	147.5	165.1	192	203.9	200.7	289.2
	Peak flow, m3/s (return period)	51.3 (<2)	87.4 (5)	74.9 (<2)	106.1 (13)	113.3 (8)	143.2 (51)	93.1 (6)
FL2*	Tide (m)	0.99	0.99	0.99	0.94	0.94	0.94	0.17
	Surge (m)	3.12	3.12	3.12	3.17	3.07	3.17	3.93
	Accumulated precipitation (mm)	128.5	147.5	165.1	192	203.9	200.7	289.2
	Peak flow, m3/s (return period)	51.3 (<2)	87.4 (5)	74.9 (<2)	106.1 (13)	113.3 (3(8))	143.2 (51)	93.1 (6)
SD1	Tide (m)	0.82	0.82	0.82	0.4	0.4	0.4	0.01
	Surge (m)	2.37	2.37	2.37	2.3	2.3	2.3	1.87
	Accumulated precipitation (mm)	24.8	24.7	21.5	17	17.7	15.1	8.9
	Peak flow, m3/s (return period)	3.4 (<2)	9.3 (<2)	3.3 (<2)	4.7 (<2)	1.3 (<2)	0.9 (<2)	0.03 (<2)
SD2	Tide (m)	1.01	1.01	1.01	1.13	1.13	1.13	-0.15
	Surge (m)	2.56	2.56	2.56	2.8	2.8	2.8	1.95
	Accumulated precipitation (mm)	24.8	24.7	21.5	17	17.7	15.1	8.9
	Peak flow, m3/s (return period)	3.4 (<2)	9.3 (<2)	3.3 (<2)	4.7 (<2)	1.3 (<2)	0.9 (<2)	0.03 (<2)
SD3*	Tide (m)	1.01	1.01	1.01	1.13	1.13	1.13	-0.15
	Surge (m)	3.12	3.12	3.12	3.4	3.4	3.4	2.5640 16
	Accumulated precipitation (mm)	24.8	24.7	21.5	17	17.7	15.1	8.9
	Peak flow, m3/s (return period)	3.4 (<2)	9.3 (<2)	3.3 (<2)	4.7 (<2)	1.3 (<2)	0.9 (<2)	0.03 (<2)
SD4	Tide (m)	1.01	1.01	1.01	1.13	1.13	1.13	-0.15
	Surge (m)	2.56	2.56	2.56	2.8	2.8	2.8	1.95
	Accumulated precipitation (mm)	555.3	546.9	526.8	338.2	330.2	316.6	323.7
	Peak flow, m3/s (return period)	242.4 (316)	319.1 (326)	201.7 (28)	178.3 (98)	168.4 (48)	197.0 (301)	94.7 (6)
SD5*	Tide (m)	1.01	1.01	1.01	1.13	1.13	1.13	-0.15
	Surge (m)	3.12	3.12	3.12	3.4	3.4	3.4	2.5640 16
	Accumulated precipitation (mm)	555.3	546.9	526.8	338.2	330.2	316.6	323.7
	Peak flow, m3/s (return period)	242.4 (316)	319.1 (326)	201.7 (28)	178.3 (98)	168.4 (48)	197.0 (301)	94.7 (6)

Formatted: Font: 9 pt, Bold, Font color: Black

Formatted: Normal, Space After: 10 pt, Border: Top: (No border), Bottom: (No border), Left: (No border), Right: (No border), Between : (No border)

Formatted: Font: 9 pt, Bold, Font color: Black

Formatted: Font: 9 pt, Bold, Font color: Black

Formatted: Font color: Black

Formatted: English (United Kingdom)

Formatted: English (United Kingdom)

Formatted: English (United Kingdom)

Formatted: English (United Kingdom)

Formatted: English (United Kingdom)

Formatted: English (United Kingdom)

Formatted: English (United Kingdom)

Formatted: English (United Kingdom)

	Tide (m)	1.16	1.16	1.16	1.1	1.1	1.1	0.93
	Surge (m)	1.94	1.94	1.35	1.42	1.42	1.42	1.1
IR1	Accumulated precipitation (mm)	187.8	177.8	173.5	98.1	91.6	86.1	58.5
	Peak flow, m3/s (return period)	158.5 (56)	201.1 (58)	126.7 (26)	93.9 (5)	85.7 (5)	93.5 (5)	30.8 (3)
	Tide (m)	1.16	1.16	1.16	1.1	1.1	1.1	2
	Surge (m)	2.54	2.54	1.94	2.03	2.03	2.03	1.7
IR2*	Accumulated precipitation (mm)	187.8	177.8	173.5	98.1	91.6	86.1	58.5
	Peak flow, m3/s (return period)	158.5 (56)	201.1 (58)	126.7 (26)	93.9 (5)	85.7 (5)	93.5 (5)	30.8 (3)

Formatted: English (United Kingdom)

Formatted: English (United Kingdom)

**Table 4: Overall extent of the inundated area (in km<sup>2</sup>), the relative difference (% change in parenthesis) compared to the FEMA 100yr Flood Zone and dCorr (correlation between differences in flood extent as compared by FEMA, and flow and surge peak)**

CI <sub>s</sub>	FL1	FL2	SD1	SD2	SD3	SD4	SD5	IR1	IR2	dCorr surge	dCorr flow
CI1	1.6 (-8.5)	1.8 (2.9)	0.9 (-48.1)	1.4 (-21.7)	1.9 (8.3)	1.7 (-2.8)	2.0 (13.9)	1.3 (-27.5)	1.5 (-15.9)	0.86	0.40
CI2	3.9 (134.2)	4.0 (139.4)	1.9 (-12.7)	2.1 (25.6)	2.3 (36.3)	3.7 (123.7)	4.8 (185.2)	1.6 (-1.9)	4.9 (192.2)	0.53	0.55
CI3	4.7 (2.6)	4.9 (7.5)	3.5 (-24.5)	4.0 (-10.5)	4.3 (-6.2)	5.4 (17.5)	7.1 (56.2)	3.2 (-29.3)	4.0 (-12.1)	0.67	0.70
CI4/CI5	2.7 (-8.3)	3.2 (8.4)	2.4 (-18.5)	2.6 (0.3)	3.4 (13.8)	2.9 (2.5)	3.6 (22.2)	2.0 (-32.3)	2.4 (-17.3)	0.98	0.43
CI6	0.9 (3.7)	0.9 (13.1)	0.7 (-14.9)	0.8 (-10.3)	1.0 (16.6)	0.9 (11.4)	1.0 (16.5)	0.7 (-20.4)	0.8 (-4.8)	0.84	0.56
CI7	2.5 (1.0)	2.7 (12.5)	1.6 (-33.9)	2.0 (-12.8)	2.6 (8.5)	2.1 (-10.7)	2.6 (7.3)	1.9 (-23.5)	2.3 (-7.5)	0.81	0.46
CI8	3.1 (4.5)	3.5 (18.4)	0.4 (-87.8)	2.1 (-28.8)	2.6 (-11.1)	2.2 (-22.3)	2.7 (-8.9)	1.1 (-63.1)	1.8 (-37.9)	0.88	0.67

Note: (-) Area inundated less than FEMA's 100yr zone

Formatted: Font: 9 pt, Bold, Font color: Black

Formatted: Normal, Space After: 10 pt, Border: Top: (No border), Bottom: (No border), Left: (No border), Right: (No border), Between : (No border)

Formatted: Width: 8.5", Height: 11", From text: 0", Numbering: Restart each page

Formatted: Font color: Black

Formatted: English (United Kingdom)

Formatted: English (United Kingdom)

Formatted: English (United Kingdom)

Formatted: English (United Kingdom)

Formatted: English (United Kingdom)

Formatted: English (United Kingdom)

Formatted: English (United Kingdom)

Formatted: English (United Kingdom)

Formatted: English (United Kingdom)

Formatted: English (United Kingdom)

Formatted: English (United Kingdom)

Formatted: English (United Kingdom)

Formatted: English (United Kingdom)

Formatted: English (United Kingdom)